Cell surface localisation of GPI-anchored receptors in *Trypanosoma brucei*

Sourav Banerjee[1*], Nicola Minshall[1*], Alexander D Cook[2,3], Olivia Macleod[1], Helena Webb[1], Matthew Higgins[2,3] and Mark Carrington[1]

[1] Department of Biochemistry, University of Cambridge, Tennis Court Road, Cambridge CB2 1QW, UK.

[2] Department of Biochemistry, University of Oxford, South Parks Road, Oxford OX1 3QU, UK.

[3]Kavli Institute for Nanoscience Discovery, Dorothy Crowfoot Hodgkin Building, University of Oxford, South Parks Rd, Oxford, OX1 3QU, UK.

* These authors made equal contributions

Correspondence: Mark Carrington: mc115@cam.ac.uk

ABSTRACT

Trypanosoma brucei, the causal agent of Human and Animal African trypanosomiasis proliferates in the extracellular milieu of mammals. It acquires host macromolecular nutrients, by receptor mediated endocytosis. The best characterised cell surface receptor is for transferrin (TfR) and it has been reported to be preferentially localised in the flagellar pocket domain of the plasma membrane, the sole site of endocytosis. In this location the TfR may be inaccessible to adaptive immune system effectors. The *T. brucei* genome encodes ~15 TfR variants, and here we compared two, the first attached to the plasma membrane by a single glycosylphosphatidylinositol (GPI)-anchor and the other by two. Transferrin uptake kinetics were similar and rapid for both. Unexpectedly, initial binding of transferrin occurred over the whole cell surface suggesting the TfR was not localised solely in the flagellar pocket. This localisation was confirmed by immunofluorescence assays and was independent of the number of GPI-anchors. Two other GPI-anchored receptors were investigated to determine whether localisation to the whole cell surface was a general property of GPI-anchored receptors. Haptoglobin-haemoglobin uptake assays and immunofluorescence localisation of complement factor H receptor showed both were also whole cell surface localised. The mechanisms by which trypanosome receptors are protected from antibody-mediated attack are more complex than hiding in a pocket.

INTRODUCTION

Trypanosoma brucei proliferates within the bloodstream and tissue spaces of mammals and can maintain a long-term infection lasting in some cases for years. To do this, it must avoid the host adaptive and innate immune response at the same time as acquiring nutrients from the host. The adaptive immune response is overcome through a population survival strategy based on a densely packed surface coat of variant surface glycoprotein (VSG) that undergoes antigenic variation. As the antibody titre against one VSG increases, a small subset of trypanosomes that have switched expression to a different VSG escape until they are recognised in turn and so on in an iterative process (Mugnier et al., 2015). The trypanosome has evolved mechanisms to increase the titre of host immunoglobin required for killing. First, there is rapid endocytosis and degradation of VSG bound antibody (Engstler et al., 2007) and second, a receptor for IgG Fc region (ISG75) (Mikkelsen et al., 2024). How the innate immune system is countered is less well understood (Pinger et al., 2018) but receptors for Complement C3, known as ISG65, and Factor H (FHR) have been identified and characterised (Cook et al., 2024; Macleod et al., 2020, 2022). Acquisition of small molecule nutrients, such as glucose and amino acids, use typical eukaryotic membrane transporters.

Obtaining host macromolecule nutrients poses a more complex problem. First, *T. brucei* has a very wide host range and presumably receptors recognise ligands from a range of host species, this has been shown to be the case for the transferrin (TfR) (Trevor et al., 2019). Second, as the TfR and haptoglobin haemoglobin receptor (HpHbR) (Lane-Serff et al., 2016) bind ligands that have similar dimensions to immunoglobulin molecules then why are host antibodies against receptors not sufficient to clear an infection? Some models to account for this suggested that the VSG coat acts as a barrier preventing immunoglobulin access. However, it was shown that antibodies could penetrate a significant distance into the VSG coat (Hsia et al., 1996) but not to the small plasma membrane proximal VSG domain (Schwede et al., 2011). Both the ligand size and the penetration of antibodies into the VSG coat made it unlikely that receptors were sterically protected from antibody binding. Immunization of mice with recombinant ISG65 or ISG75 did not protect against infection (Ziegelbauer & Overath, 1993). In addition, accessibility of the HpHbR was demonstrated by the ability of a monoclonal antibody drug conjugate to clear infections in a mouse model (MacGregor et al., 2019).

The trypanosome flagellar pocket is an invagination of the plasma membrane at the base of the single flagellum and is the sole site of endo- and exocytosis. The location of the flagellar

pocket at the posterior end of the cell is central to the mechanism of clearance of immunoglobulin molecules bound to VSG. The forward swimming motion of the trypanosome exerts a hydrodynamic force on the immunoglobulin that protrudes above the top of the VSG coat pushing the antibody-VSG complex towards the flagellar pocket and subsequent endocytosis (Engstler et al., 2007). Since the hydrodynamic flow requires only binding to a cell surface protein, it is likely to occur with any large ligand bound to a receptor providing it has free lateral movement in the plane of the membrane. The flagellar pocket is a discrete domain of the plasma membrane (Gadelha et al., 2009) with several exclusively localised proteins (Gadelha et al., 2015). At the neck of the pocket, there is a restriction introduced by close contact between the plasma membranes of the flagellum and pocket as it emerges onto the cell body. This flagellar pocket collar is maintained by specific proteins (Bonhivers et al., 2008)(Gadelha et al., 2009). The exclusive localisation of some proteins to the plasma membrane of the flagellar pocket, others to the cell body, and a range to both, indicates that there is regulated passage between the two domains of the plasma membrane.

There is variation in the reported localisation of receptors to different domains of the plasma membrane. TfR was the first receptor to be identified, it is glycosylphosphatidylinositol (GPI)-anchored and has been localised to the flagellar pocket and endosomal membrane in some studies but others suggested it was on the flagellar pocket, cell body plasma membrane and endosomal membrane (Duncan et al., 2024; Mussmann et al., 2003, 2004; Steverding et al., 1994a, 1995; Tiengwe et al., 2017). The Complement Factor H receptor (FHR) is a monomer probably GPI-anchored and is localised to the cell body and flagellar plasma membrane (Macleod et al., 2020). HpHbR, also probably GPI-anchored, has been localised to the flagellar pocket (Vanhollebeke et al., 2008). Reporter proteins with a single GPI-anchor are also present on the cell body plasma membrane (Schwartz et al. 2005). ISG65 and ISG75 are type I transmembrane proteins and localise to the flagellar, cell body, and pocket plasma membrane as well as the endosome (Leung et al., 2011; Ziegelbauer et al., 1992). The localisation of receptors to the flagellar pocket has been proposed to protect the cell from downstream effects of antibody recognition of the receptor but the discovery of new receptors, such as Complement C3 binding by ISG65 (Macleod et al., 2022) and FHR (Macleod et al., 2020) that are more abundant and distributed over the cell surface seems to contradict this argument.

Newly synthesised or recycled proteins are added to the plasma membrane at the flagellar pocket. Some proteins are retained in the flagellar pocket and have limited or no distribution over the cell surface (Billington et al., 2023). It is assumed that these proteins have a

retention and/or retrieval signal. For transmembrane proteins a signal could be in the cytoplasm. In contrast, GPI-anchored proteins have no cytoplasmic component and recognition must occur on the external face of the plasma membrane. Any signal for retention has to operate in a background of sequence variation in VSGs which makes short amino acid motifs unlikely. TfR is a heterodimer with the two subunits, ESAG6 and ESAG7, forming a single binding site for monomeric transferrin. ESAG6, but not ESAG7, has a GPI-anchor so the TfR is tethered to the plasma membrane by a single anchor in contrast to VSG dimers and trimers which have a GPI-anchor on each subunit. There is experimental evidence that the signal for TfR concentration in the flagellar pocket is the number of GPI-anchors per molecule, a single anchor leading to a greater retention, and more than one anchor ready to escape to the surface of the cell body (Schwartz et al., 2005; Tiengwe et al., 2017). These experiments manipulated the number of GPI-anchors on TfR, heterodimer with a single anchor on one subunit. Adding an anchor to the second subunit caused a change in localisation to the cell surface and endosome as judged by immunofluorescence. However, conditions that led to a few fold increase in expression of single GPI-anchored TfR, including transferrin shortage and growth at high cell density, resulted in the detection of TfR on the cell body surface (Mussmann et al., 2004). Whether the surface-localized TfR is functional remains unproven (Mussmann et al., 2004; Schwartz et al., 2005).

TfR is encoded by a dispersed gene family with ~15 TfR variants. The experiments here started with a chance observation that one of these encoded a receptor with two GPI-anchors while the others have a single anchor. This was exploited to investigate how the presence of one or two GPI-anchors affected function. We show that the second GPI-anchor has no effect on the kinetics of uptake, or processing of transferrin through the endosome. However, the second anchor resulted in ≥1.5-fold increase in steady state receptor levels. Further, transferrin uptake experiments provided evidence that TfR was present over the entire cell surface and this was supported by immunofluorescence experiments. An analysis of the localisation of two other putatively GPI-anchored proteins showed that all were present over the entire cell surface. These experiments demonstrate that the trypanosome expresses a set of receptors over the entire cell surface inferring that there are effective mechanisms to resist antibody mediated recognition of conserved cell surface proteins.

RESULTS

The BES7 VSG expression site encodes a transferrin receptor with two GPI-anchors

166 In *T. brucei*, the active VSG gene is transcribed from a bloodstream form expression site
167 (BES) that is telomere proximal. BESs contain up to 12 other co-transcribed expression site
168 associated genes (ESAGs) (Hertz-Fowler et al., 2008; Pays et al., 2001). TfRs are
169 heterodimers encoded by ESAG6 and ESAG7 (Chaudhri et al., 1994; Salmon et al., 1994a)
170 The ESAG6 and 7 subunits share around 80% amino acid identity although ESAG6 has an
171 additional 24 residues at the C-terminus preceding a GPI-anchor addition signal. Different
172 BESs encode variants of ESAG6 and 7 with 90% or more amino acid sequence identity
173 (Maier & Steverding, 2008; Trevor et al., 2019). In *T. brucei* Lister 427, the isolate used in
174 these experiments, there are 15 BESs (Barcons-Simon et al., 2023) and most were
175 sequenced and annotated after transformation associated recombination cloning of
176 telomeres (Hertz-Fowler et al., 2008). In the original annotation, BES7 stands out as it has
177 two copies of ESAG6 but apparently lacked ESAG7 and as such would not be able to make
178 a functional TfR. Here, a fresh analysis of the sequence was performed and indicated that
179 the first 'ESAG6' gene annotated in BES7 actually encoded an ESAG7 with a C-terminal
180 extension and a GPI-anchor typical of an ESAG6. In addition, there was a second ESAG6
181 gene (ESAG6.2) downstream of the annotated copy (ESAG6.1), the two copies encode
182 proteins with a single difference in 401 residues (M110->V). Phylogenetic analysis of ESAG6
183 and ESAG7 confirmed that a copy of ESAG7 is indeed present in BES7 along with a single
184 copy of ESAG6 (Figure 1A).
185
186 The origin of the GPI-anchor attachment signal in BES7 ESAG7 was investigated by
187 comparing the ESAG7 mRNA sequences from 13 different BESs. This showed that all the
188 ESAG7 genes contained residual coding sequences for GPI-anchor addition but a set of
189 small deletions between nucleotides 985 and 1068 in the ORF resulted in a frameshift
190 leading to a premature stop codon at the C-terminal end effectively removing the GPI-anchor
191 attachment sequence (Figure S1). A comparison of BES7 ESAG6 and 7 showed that the C-
192 terminal 120 amino acid sequences are identical and there was a clear prediction for a GPI-
193 anchor on both using NetGPI 1.1 (Gíslason et al., 2021) (Figure S2).
194
195 **Cellular TfR protein levels are determined by BES identity and the number of GPI-**
196 **anchors**
197
198 ESAG6 and 7 protein levels were examined by western blotting in cell lines expressing
199 VSGs and TfRs from three different BESs: BES3-VSG118, BES1-VSG221 and BES7-
200 VSG224 (Figure 1B). TfRs have several N-linked glycosylation sites and whole cell lysates
201 were treated with PNGaseF to simplify analysis. First, in BES7 cells there was a shift in the
202 apparent molecular weight of ESAG7 from ~30 kDa to ~38 kDa, which is consistent with the

203 addition of a GPI-anchor (Figure 1B), such a change in mobility on the addition of a GPI-
204 anchor to ESAG7 has been reported previously (Tiengwe et al., 2017). Second, the identity
205 of the active BES affected both ESAG6 and ESAG7 protein levels, there were increasing
206 levels of expression: BES3 < BES1 < BES7 (Figure 1B). Lastly, when the BES7 cell line was
207 modified to exchange VSG224 to VSG221 (see below), this had little effect on TfR
208 expression, suggesting the BES identity was the dominant determinant rather than the VSG
209 type. The rabbit TfR antiserum used was raised against the TfR from BES1 (Gerrits et al.,
210 2002) and is the same as used in most other studies (Mussmann et al., 2003; Tiengwe et al.,
211 2017). The amino acid sequence identity between BES2 TfR and BES1 TfR is >98% and
212 BES7 TfR is >92% and it is unlikely that the difference in TfR levels result from differential
213 reactivity of the serum to different TfRs. Support for the different levels of TfR expression
214 was obtained when the levels of TfR mRNAs were estimated in the BES3, BES1 and BES7
215 cell lines using RNAseq (Table S1). The level of TfR mRNAs were expressed as a ratio
216 (ESAG6+ESAG7):VSG and were consistent with the differences seen in protein levels
217 (BES3, 0.022 < BES1, 0.038 < BES7, 0.077).
218
219 We next investigated whether GPI-anchor number contributed to the variation in cellular TfR
220 levels by making a set of transgenic cell lines (Figure 2A). First, VSG224 in BES7 was
221 changed to VSG221. Next, the cell line expressing VSG221 from BES7 was modified to alter
222 the ESAG7 by exchanging the 3' end of the ORF with that from BES1 ESAG7 resulting in
223 the loss of the GPI-anchor signal. As a control, a second cell line in which the ESAG7 gene
224 retained the GPI-anchor addition sequence was made. Similar modifications were performed
225 on cells expressing VSG221 from BES1, cell lines expressing either BES1 ESAG7 modified
226 with the C-terminal GPI-anchor sequence from BES7 ESAG7 or the endogenous BES1
227 ESAG7 were made. The result was four cell lines: all expressed VSG221 from either BES1
228 or BES7 and TfR with or without a GPI-anchor on ESAG7.
229
230 The cell lines were characterised by western blotting of PNGaseF-treated whole cell lysates
231 (Figure 2B). The addition of a GPI-anchor signal sequence to ESAG7 resulted in an increase
232 in both ESAG6 and 7. To estimate this change, whole cell lysates were minimally separated
233 by SDS-PAGE to collapse the ESAG6 and 7 proteins into a single band prior to western
234 blotting. Relative quantitation was obtained using a titration curve of the highest TfR
235 expresser and normalised against SCD6 for loading (Figure 2C). Three biological replicates
236 were performed and the levels of both TfRs from BES1 is significantly lower ($p<0.01$), ~3.5
237 fold, compared to BES7, regardless of GPI-anchor number. The presence of a GPI-anchor
238 on ESAG7, leading to a double-anchored TfR, significantly increased ($p<0.05$) the
239 expression level by approximately 1.9-fold in BES1 and about 1.5-fold in BES7. This

240 provides strong evidence that the presence of a GPI-anchor on ESAG7 contributes to the
241 higher cellular expression level of TfR, which could result from increased protein stability,
242 reported for VSGs, (Bangs et al., 1986; Engstler et al., 2004) or a higher rate of turnover
243 and/or greater shedding of the single GPI-anchored TfR (Schwartz et al. 2005).
244
245 **Transferrin uptake kinetics are similar in cells expressing TfRs with either one or two**
246 **GPI-anchors**
247
248 To investigate whether anchor number influenced function, BES7-VSG221 cell lines
249 expressing single or double GPI-anchored TfR were used. It has already been shown that a
250 TfR with double GPI-anchors is functional (Tiengwe et al., 2017), here the kinetics of
251 transferrin binding and uptake by single and double GPI-anchor TfRs were compared. The
252 experimental approach was similar to that developed to characterise the binding and
253 endocytosis of VSG antibodies (Engstler et al., 2007). The medium used to culture
254 trypanosomes contained ~2.5 μM transferrin (Kakuta et al., 1997), Alexa 568 labelled bovine
255 holo-transferrin (Tf_{A568}) was added to cultures, without any other manipulation, to a final
256 concentration of 0.5 μM (so that 1 in 6 molecules of Tf In the medium is now fluorescent)
257 and cells were then fixed over a time course from 15 to 600 seconds and imaged by
258 epifluorescence microscopy (Figure 3A and S3A). The on rate for binding of Tf to TfR is very
259 rapid (4.5×10^5 $M^{-1}s^{-1}$ at pH 7.4 for BES1 TfR and bovine Tf) (Trevor et al., 2019) and
260 binding will occur to unoccupied receptor almost immediately. At 15 seconds there was
261 variation between individual cells with Tf_{A568} present on the flagellum, across the cell body
262 and the flagellar pocket in both cell lines. There was also variation at 60 seconds, Tf_{A568} was
263 present in the endosomal compartment of most cells, and the cell surface in some cells. At
264 600 seconds the Tf_{A568} was predominantly within the endosomal compartment. The variation
265 was also examined by quantifying the fluorescence from individual cells (Figure 3B), this
266 showed the range of variation and an increase in fluorescence between 15 and 60 seconds
267 followed by a decrease by 600 seconds. Fluorescence intensity was also determined across
268 transverse sections of the cell (Figure 3C), this showed some cells with internal signal and
269 others with two peaks consistent with a cell surface localisation. There was a stronger signal
270 from cells expressing TfR with two GPI-anchors, consistent with higher expression levels,
271 but no consistent differences in distribution were seen.
272
273 The same Tf_{A568} uptake assay was performed with the BES1-VSG221 cells expressing TfRs
274 with one or two GPI-anchors (Figure 3D and S3B). There was a reduced binding and uptake
275 of Tf_{A568} in BES1 cells compared to BES7 cells as might be expected given lower levels of

276 the receptor. Otherwise, the time course of uptake was similar: at 15 seconds Tf_{A568} was
277 present on the flagellum and cell body surface as well as the flagellar pocket in both cell
278 lines, at 60 seconds Tf_{A568} on the cell surface was reduced and some was now present in the
279 flagellar pocket and endosomal compartments, and by 600 seconds Tf_{A568} was substantially
280 within endosomal compartments. In both BES7 and BES1 cell lines, fluorescence distribution
281 patterns across the cells showed variability at 15 and 60 sec (Figure 3E-F), but appeared
282 more uniform at 600 sec.
283
284 Previous studies have shown that some TfRs do not bind canine transferrin (Mussmann et
285 al., 2003). Canine transferrin has 501/686 amino acid sequence identities with bovine
286 transferrin (Figure S4A) and it was used as a negative control in the same transferrin binding
287 and uptake assay above using BES7-VSG221 cells expressing TfR with either one or two
288 GPI-anchors (Figure S4B). No cell binding or uptake of canine Tf in either cell line was
289 observed. In addition, a competition assay for binding of fluorescent Tf was performed by
290 adding 5- or 10-fold excess of unlabelled Tf at the same time (Figure S4C). The signal from
291 labelled Tf was reduced by the competition indicating saturable binding, consistent with a
292 receptor mediated process. These findings provide evidence that the binding of bovine
293 transferrin to the cell surface is receptor dependent. An important point is that fluorescent Tf
294 was added to cells in culture without any other manipulation as preliminary experiments
295 indicated that centrifugation, washing and resuspension in medium led to a reduction in
296 cellular TfR for up to 2 hours (Figure S4D).
297
298 Together, these experiments support a model in which the TfR is present on the cell surface,
299 and endocytosis is a rapid process. The greater Tf binding and uptake in BES7 compared to
300 BES1 cells provides evidence that TfR abundance limits the amount of Tf endocytosed. The
301 number of GPI-anchors on the TfR has no obvious influence on Tf uptake but does affect
302 receptor levels.
303
304 The finding that Tf_{A568} was bound over the whole cell surface at early time points in the
305 uptake assays suggested a similar localisation for the TfR. This is not consistent with some
306 previous studies that found TfR and other GPI-anchored receptors sequestered in the
307 flagellar pocket (Duncan et al., 2024; Mussmann et al., 2004; Steverding et al., 1994a, 1995;
308 Tiengwe et al., 2017; Vanhollebeke et al., 2008) or that expression level determined
309 localisation (Mussmann et al., 2003). We went on to characterise the cellular localisation of
310 single and double GPI-anchored TfR along with two other GPI-anchored receptors.
311
312 **Localisation of the transferrin receptor by immunofluorescence**

313

314 Previous reports provided evidence that in BES1-VSG221 cells grown in the presence of
315 10% FBS, the cell surface TfR is located or concentrated within the flagellar pocket and
316 endosome, rather than dispersed on the cell body (Ligtenberg et al., 1994; Mussmann et al.,
317 2003; Salmon et al., 1994a; Tiengwe et al., 2017). In contrast, when cells are treated to
318 increase TfR expression by roughly three to fivefold, for example when grown to high density
319 or in canine serum, TfR localizes on the cell body (Mussmann et al., 2003). To resolve this
320 discrepancy, the localisation of the TfR was investigated using immunofluorescence. Based
321 on the transferrin uptake experiments, we reasoned that the localisation of the TfR would be
322 very dynamic and thus chose to fix the cells in culture without any centrifugation or washing,
323 this approach was supported by preliminary experiments comparing protocols (Figure S5A-
324 B) that showed both the composition of the fixative and absence of a washing step altered
325 the outcome.

326

327 Four cell lines, BES1-VSG221 and BES7-VSG221 cells each expressing TfR with one or two
328 GPI-anchors, were investigated. Fixative was added to cells in culture without any other
329 manipulations, the final concentrations were 4% formaldehyde and 0.2% glutaraldehyde and
330 TfR localisation was observed by immunofluorescence after settling cells on microscope
331 slides. Under these experimental conditions, the TfR in all four cell lines had a distribution
332 across the entire cell surface including the flagellar pocket and in internal compartments in
333 some cells (Figure 4A). Fluorescence intensity measurements across transverse sections of
334 both the BES7 1- and 2 GPI cells confirmed that TfR is indeed present on the surface of
335 some cells as seen by two peaks in fluorescence corresponding to the cell periphery in some
336 cells (Figure 4B). As in the Tf uptake experiments, the strength of signal as measured by
337 total fluorescence intensity from individual cells showed that TfR abundance varied between
338 individual cells in populations (Figure 4C and Figure S5C). These measurements also
339 showed that the presence of two GPI-anchors on TfR increased levels by about 1.5-fold
340 compared to the single anchored receptor and that there is a ~3.5-fold higher TfR
341 expression in BES7 compared to BES1 cells regardless of GPI-anchor number. These
342 measurements support the western blot quantitation (Figure 2) and also provide evidence
343 that the immunofluorescence signal does not contain a significant level of non-specific
344 background.

345

346 Structured Illumination Microscopy (SIM) was used to obtain more information on TfR
347 localisation in the same four cell lines as above (Figure 5). TfR was present on the cell
348 surface including the flagellar pocket, cell body and flagellum, and in the endosome (single

349 stack images) (Figure 5A). Three-dimensional reconstruction of the localization of TfR
350 confirmed that it is distributed across the cell surface and in endosomes (Figure 5B).
351
352 These experiments collectively provide strong evidence that TfR is indeed present on the *T.*
353 *brucei* cell surface under normal growth conditions and that the localization pattern is
354 independent of the presence or absence of a GPI-anchor in the ESAG7 subunit.
355
356 **Cell surface localisation is shared by two other GPI-anchored receptors**
357
358 The finding that TfR is distributed over the whole cell surface led to an investigation of other
359 receptors. Two were selected on the basis of being predicted to have one or more GPI-
360 anchors and a non-expressing negative control being available. The first was the
361 haptoglobin haemoglobin receptor (HpHbR) for which +/+ and -/- cell lines were used. The
362 structure of most of HpHbR is known and it is a monomer in solution but two or more
363 receptors can bind a single ligand (Higgins et al., 2013; Lane-Serff et al., 2014). HpHbR has
364 a low copy number, 300 to 400 per cell (Vanhollebeke et al., 2008) and, in the absence of a
365 suitable antibody, a ligand uptake assay was used. The second receptor analysed was the
366 complement factor H receptor (FHR), this was used after a fortuitous observation that
367 although it is not expressed when cells are grown in medium containing 10% foetal bovine
368 serum (Macleod et al., 2020), it is expressed at high levels when the same cells are grown in
369 medium with 10% rabbit serum replacing the foetal bovine serum. The structure of FHR is
370 known and it is a monomer with a single GPI-anchor (Macleod et al., 2020).
371
372 Alexa 568-labelled HpHb ($HpHb_{A568}$) was used in uptake assays with HpHbR +/+ and -/-
373 cells as for transferrin uptake (Figure 6A). There was binding of ligand to the cell surface by
374 15 seconds, uptake into the endosome by 60 seconds, and a location consistent with the
375 lysosome by 600 seconds. Binding and uptake were not detected in HpHbR -/- cells (Figure
376 6A). The kinetics of uptake were similar to those for transferrin. Presence of $HpHb_{A568}$ on the
377 cell surface was confirmed by the fluorescence signal measurement across the cells at 15
378 seconds, which showed two distinct peaks consistent with peripheral localisation for some
379 cells (Figure 6B), the noise in the quantification is due to the low copy number of the
380 receptor. Again, there was variability in binding and uptake of HpHb across the population
381 (Figure S6).
382
383 In trypanosomes cultured in medium containing 10% rabbit serum, expression of the FHR
384 was readily detected whereas in medium containing foetal bovine serum (FBS) it is not
385 (Figure 7A). Cells cultured with rabbit serum were used to determine the localisation of FHR

386 by immunofluorescence following the same procedure used for the transferrin receptor
387 (Figure 7B). The FHR was clearly localised over the entire cell surface. Two controls for
388 specificity of antibody binding were performed: first cells were grown in medium
389 supplemented with foetal bovine serum and second with a no primary antibody control for
390 the cells grown with rabbit serum to control for cell surface immunoglobulin originating from
391 the growth medium. Neither control gave a signal (Figure S7). SIM analysis further provided
392 spatial resolution along with reconfirming the distribution of the FHR across the trypanosome
393 cell surface and flagellum as well as within the flagellar pocket (Figure 7C).
394
395 These experiments show that the detection of TfR on the cell surface is part of a general
396 pattern where GPI-anchored receptors are distributed across the cell body plasma
397 membrane.
398
399 **DISCUSSION**
400
401 Any pathogen that has evolved to establish and maintain a long-term infection within a
402 mammalian host must be able to acquire nutrients as well as be resistant to both the innate
403 and adaptive immune responses of the host. African trypanosomes have evolved a strategy
404 that is dependent on variant surface glycoprotein (VSG), a superabundant protein that forms
405 a densely packed coat on the cell surface. Low frequency switching to a different VSG
406 allows the population to persist (Mugnier et al., 2015). The VSG coat appears to prevent
407 antibodies, and possibly innate immunity factors, gaining immediate access to the plasma
408 membrane (Schwede et al., 2011). However, such a coat cannot be totally impermeable as
409 trypanosomes require host macromolecules such as transferrin and haptoglobin-
410 haemoglobin which they acquire through receptor mediated endocytosis (Lane-Serff et al.,
411 2014; Salmon et al., 1994b; Steverding et al., 1994b, 1995; Trevor et al., 2019; Vanhollebeke
412 et al., 2008).
413
414 Why these receptors do not result in the trypanosomes becoming susceptible to immune
415 recognition and attack is central to understanding the mechanisms of infection (Banerjee et
416 al., 2024). One model proposed that the receptors are sequestered in the flagellar pocket, an
417 invagination of the plasma membrane at the base of the flagellum, and are not accessible to
418 immune effectors. The idea that sequestration in the flagellar pocket allowed receptors to
419 hide from host immune effectors was first challenged by the discovery of invariant surface
420 glycoproteins (ISGs) (Ziegelbauer et al., 1992; Ziegelbauer & Overath, 1992) that were
421 shown to be distributed over the whole cell surface (Macleod et al., 2022; Ziegelbauer &
422 Overath, 1993). Two ISGs were subsequently identified as receptors, one for complement

423 C3 and another for the Fc region of immunoglobulins (Macleod et al., 2022; Mikkelsen et al.,
424 2024). Both the ability to access ligands and the structures of the extracellular domains of
425 both ISGs indicated that they were unlikely to be physically shielded by the VSG coat. The
426 ISGs are type 1 transmembrane proteins with a large extracellular domain, a single
427 transmembrane pass and a small cytoplasmic tail. In contrast, VSGs have two or more GPI-
428 anchors whereas the two characterised nutrient receptors have a single GPI-anchor. Could
429 this difference in GPI-anchor number result in selective retention of nutrient receptors in the
430 flagellar pocket (Tiengwe et al., 2017) as it is difficult to envisage a requirement for any
431 amino acid sequence motifs in the context of variation of VSGs.
432
433 Here, we have investigated the distribution of GPI-anchored receptors on the cell surface of
434 mammalian infective *Trypanosoma brucei*. The main findings are: (1) The majority of TfRs
435 encoded in the genome have a single GPI-anchor but there is at least one with two GPI-
436 anchors. (2) The single anchored TfRs probably arose from loss of one anchor as opposed
437 to gain in the double anchored version. The loss of the GPI-anchor from ESAG7 may
438 provide a selective advantage possibly reducing exposure to the host adaptive immune
439 system without affecting transferrin acquisition (Trevor et al., 2019). (3) The steady state
440 level of TfR varies with the identity of the transcribed BES. (4) Single or double anchored
441 TfRs bind transferrin, as previously reported (Tiengwe et al., 2017) and result in similar
442 kinetics of transferrin uptake, with movement from the cell surface to the endosome
443 occurring within two minutes. The rapid kinetics of uptake indicates the receptor ligand
444 complex is probably subject to the same hydrodynamic forces as antibody VSG complexes
445 (Engstler et al., 2007) resulting in a directional movement towards the posterior end of the
446 cell, the location of the flagellar pocket and endocytosis. (5) Adding a second GPI-anchor to
447 a TfR resulted in a ~1.5-fold increase in cellular receptor levels. (6) Both single and double
448 GPI-anchored TfRs are present over the whole cell surface as seen by both transferrin and
449 antibody binding. (7) Two other GPI-anchored receptors, the HpHbR and FHR, both
450 probably with a single GPI-anchor, are present over the whole cell surface.
451
452 The earlier findings that the TfR, and subsequently the HpHbR, are localised to the flagellar
453 pocket is an attractive model as it provided an easy explanation for why the receptors did not
454 result in immune attack. The experiments presented here do not agree with this model and it
455 is worth discussing the reasons why these experimental differences have arisen. Here the
456 cells were fixed in culture using formaldehyde and a higher concentration (0.2%) of
457 glutaraldehyde than in previous reports. In contrast, much of the previous work involved
458 manipulations of the trypanosomes before determining either transferrin binding or TfR/
459 HpHbR localisation by immunofluorescence. The most common is centrifugation and

460 washing prior to fixation for immunofluorescence (Engstler et al., 2004; Roggy & Bangs,
461 1999; Tiengwe et al., 2017; Vanhollebeke et al., 2008), a process that is slow when
462 compared to the very rapid endocytosis of surface bound transferrin (Figure 3) and providing
463 time for the ligand bound receptors to be cleared from the cell surface. This would be even
464 more apparent if the experimental manipulation reduced the export of new or recycled TfRs
465 to the cell surface. An example of how protocols determine outcomes is the variation in the
466 measured half-life of TfR, which ranges from ~40 min to 7 hrs depending on the different
467 experimental protocols used (Biebinger et al., 2003; Kabiri & Steverding, 2000; Mussmann et
468 al., 2004; Tiengwe et al., 2017).
469
470 The experiments involving transferring BES1-VSG221 cells to medium in which FBS had
471 been replaced by canine serum (Mussmann et al., 2003) are informative. The BES1 TfR
472 does not bind canine transferrin and cell proliferation arrested. After ~5 days, proliferating
473 cells appeared in the culture having switched BES and thus TfR orthologue to one able to
474 bind canine transferrin (van Luenen et al., 2005). In addition, supplementing the canine
475 serum based medium with bovine transferrin prevented arrest of proliferation indicating that
476 it was due to lack of transferrin alone (Mussmann et al., 2004). In contrast to experiments
477 that wash cells into solutions that do not support growth, the transfer of BES1-VSG221 cells
478 to medium with canine serum starves the cells of just transferrin. On transfer from FBS to
479 canine serum, the TfR abundance increased 4 to 5-fold and the receptor was present all
480 over the cell surface (Mussmann et al., 2003). It is unlikely that the distribution of TfR on the
481 cell surface results from a retention system being overwhelmed given the variation in TfR
482 expression observed from different BESs (Figure 1) but is due to an absence of ligand-
483 mediated uptake. Different TfRs have a wide range of affinities for transferrins (K_D from as
484 low as 1.4 nM to >5 μM) (Trevor et al., 2019) and there will be an equilibrium with the
485 relative amounts of TfR on the cell body surface compared with the flagellar pocket and
486 internal structures that will vary with the identity of the TfR and the identity and concentration
487 of transferrin.
488
489 The experiments here were informed by the kinetics of rapid transferrin uptake (Figure 3 and
490 as an unpublished observation in (Mussmann et al., 2004) and we did not manipulate the
491 cells before ligand uptake experiments or prior to fixation for immunolocalization. The result
492 was clear evidence that TfR is expressed over the whole cell surface and is not restricted to
493 the flagellar pocket. This was reinforced by the localisation of the HpHbR and FHR, both of
494 which are monomeric (Lane-Serff et al., 2014; Macleod et al., 2020), contain a single GPI-
495 anchor, and are also present over the whole cell surface. We also observed variation in TfR
496 and HpHbR abundance between individual cells, as has been seen previously for TfR

497 (Duncan et al., 2024; Steverding et al., 1994b), and this suggests sensitivity to the
498 requirements at the individual cell level. Whether this relates to cell cycle stage or any
499 developmental progression remains to be investigated. The expression of the TfR is
500 sensitive to the availability of Fe^{3+} with a several fold increases in mRNA and protein induced
501 by iron chelators (Gilabert Carbajo et al., 2021). Growth in medium dependent on rabbit
502 serum resulted in high levels of expression of the FHR, this could result from a factor in
503 rabbit serum inducing expression or failure to bind ligand.
504
505 The findings here still leave the question of how the trypanosome avoids receptor antibody-
506 based clearance by the host immune system? Vaccination of mice with ISGs did not result in
507 any protection (Ziegelbauer & Overath, 1993), this shows that receptors do not have to be
508 sequestered in the flagellar pocket to avoid the host adaptive immune system. The effective
509 killing of trypanosomes by antibody-drug conjugates recognising the HpHbR shows that
510 receptors are accessible (MacGregor et al., 2019), as does inhibition of transferrin binding by
511 Fab fragments (Steverding et al., 1995). It is likely that a combination of processes results in
512 resistance to receptor antibody-mediated killing: first antibodies have to recognise parts of
513 the receptor that are accessible in the VSG coat, this will be affected by the structure of the
514 receptor and how much is occluded by ligand binding, a function of ligand concentrations,
515 host species and receptor K_D. Enough antibody has to be present on the cell surface for long
516 enough to elicit a response. Two factors affect this, first the copy number of the receptor,
517 ISGs are present at 50,000 to 70,000 per cell (Ziegelbauer et al., 1992) (<1% of VSG), TfR
518 at a few thousand, but variable (Steverding et al., 1995), and HpHbR at 300 to 400
519 (Vanhollebeke et al., 2008). Second, the half time of the receptor antibody complex on the
520 cell body plasma membrane will be short (Steverding et al., 1995) as the hydrodynamic
521 forces rapidly push VSG-antibody complexes toward the flagellar pocket and endocytosis
522 (Engstler et al., 2007). In summary, we provide evidence that GPI-anchored receptors in
523 trypanosomes are not sequestered in the flagellar pocket but are distributed across the cell
524 body and flagellum surface plasma membrane and this leads to re-evaluation of how
525 trypanosomes avoid receptor antibody mediated clearance.
526
527
528 **MATERIALS AND METHODS**
529
530 **Cell lines**
531 *T. brucei* Lister427 bloodstream form cell lines were used throughout expressing either
532 VSG221 (MiTat1.2) from BES1, VSG118 (MITat 1.5) from BES3 or VSG224 (MITat 1.3) from

533 BES7. BES7 expressing cells were as described in Hertz-Fowler *et al.* (Hertz-Fowler et al.,
534 2008) where BES1 and BES7 were tagged with Puromycin and G418 resistance genes
535 respectively. Cells were maintained in culture in HMI-11 medium (Hirumi & Hirumi, 1989).
536 For ligand-uptake assays and immunofluorescence cells were harvested in mid-log phase
537 (0.5-1x10^6 cells/ml). To allow further modification by (CRISPR)-associated gene 9 (Cas9)
538 gene editing, BES1 and BES7 expressing cell lines were first modified by transfection with a
539 construct containing Cas9 and T7 RNA polymerase transgenes (Beneke et al., 2017).
540 Antibiotic selection was used when appropriate. The primers used to generate the cell lines
541 are listed in Table S5.
542
543 **Constructs for ESAG7 +/- GPI attachment site**
544 Constructs are represented schematically in Figure 2A and described in brief below:
545 BES7 constructs:
546 The presence of a G418 resistance gene upstream of ESAG7 was utilised to generate the
547 required constructs from BES7 genomic DNA (Hertz-Fowler et al., 2008). A PacI-EcoRI PCR
548 fragment from the promoter to the G418 resistance gene start was annealed to an EcoRI-
549 PacI PCR fragment from the G418 stop codon through to the ESAG7 3' UTR. The resulting
550 EcoRI site was used to insert a blasticidin resistance open reading frame. The entire
551 construct was cloned into pGEM-T, allowing the required cassette to be excised by PacI for
552 transfection into BES7 cells expressing Cas9, alongside suitable sgRNAs to target the
553 BES7-ESAG7 region, designed by ChopChop (https://chopchop.cbu.uib.no/). This construct
554 contained the endogenous BES7 ESAG7 including its GPI anchor. To remove the GPI
555 anchor addition sequences and express an ESAG7 similar to those in the other Lister427
556 bloodstream expression sites, a SacI-BsrBI fragment was excised and replaced with the
557 corresponding fragment from BES1 ESAG7. This fragment was generated by RT-PCR from
558 RNA isolated from BES1 VSG221 cells using standard methods.
559 BES1 constructs:
560 A similar approach was used to make ESAG7 modifying constructs from BES1 exploiting a
561 puromycin resistance gene located between the promoter and the ESAG7 gene in the BES1
562 expression site (Hertz-Fowler et al., 2008). PacI-BstEII and BstEII-PacI PCR fragments were
563 generated from genomic DNA, ligated and cloned into pGEM-T. To generate BES1-ESAG7
564 with a GPI anchor from the BES1 expression site, the distal SacI-PacI fragment was
565 replaced by a PCR fragment encoding SacI-ESAG7 stop codon (blunt end) from BES7-
566 ESAG7 DNA and a BES1-ESAG7 3' UTR region from the BES1 site corresponding to the
567 BES7-ESAG7 stop codon (blunt end) to PacI. Constructs were linearised with PacI and
568 transfected with sgRNAs targeting the ESAG7 gene in either BES7 or BES1 and

electroporated into BES1 VSG221 cells expressing Cas9. BES7 modified cell lines were selected with blasticidin and BES1 modified cell lines with puromycin.

Changing the VSG from 224 to 221:

BES7-VSG224 expression was switched to VSG221 by transfection of a linearised plasmid fragment encoding VSG221, flanked by 5' and 3' VSG221 intergenic regions and a downstream G418 resistance gene flanked by alpha-beta tubulin intergenic regions. Sequences targeting the 5' and 3' UTRs of the endogenous VSG224 gene were generated by PCR from BES7 (TAR153) DNA (a kind gift of Luísa Figueiredo) and cloned via KpnI/XhoI and SpeI/SacI fragments upstream and downstream of the VSG221-blasticidin expression cassette. G418 resistant clones were screened for binding to anti-VSG221 antibody through immunofluorescence assays and confirmed by Western blot analysis.

Protein gel electrophoresis and Western blotting

Protein samples were prepared and analysed by SDS-PAGE and western blotting following standard methods. Briefly, cells were harvested by centrifugation, washed in serum-free HMI-9 and resuspended in Protein Sample Buffer (10% glycerol, 2% w/v SDS, 80 mM Tris-HCl pH 6.8), at a concentration of $2x10^8$ cells/ml. Immobilon-P membrane (Millipore) was used to retain the proteins. The primary antibodies used during western blotting are rabbit anti-FHR (Macleod et al., 2020) and rabbit anti-TfR (a kind gift of Piet Borst). Polyclonal anti-VSG221 and anti-SCD6 antibodies were generated from recombinant *E. coli* expressed proteins, injected into rabbits by standard methods (Covalab). Secondary antibodies used were Peroxidase-conjugated AffiniPure Goat Anti-Rabbit IgG (H+L) (Jackson Immunoresearch) and Alexa Fluor 488-Donkey Anti-Rabbit IgG (H+L) (Invitrogen). Membranes were blocked in Tris-buffered saline (TBS), 0.1% Tween20, 2% w/v Marvel dried milk and probed in appropriate dilutions of primary and secondary antibodies. Washing steps were performed with TBS, 0.1% Tween20 and blots were analysed on a BioRad ChemiDoc system, ensuring signals remained below saturation limits. Quantitation of transferrin receptor protein level was performed using Fiji-ImageJ software (https://imagej.net/software/fiji/), with background subtraction and comparison with intensity measurements taken from a protein dilution series from BES7 expressing cells.

RNAseq

mRNA was sequenced using Illumina paired-end sequencing technology by the Beijing Genomics Institute. Raw reads were deposited to ENA under the accession number PRJEB90063. Analysis was perfomed using Galaxy (www.usegalaxy.org) (Afgan et al., 2018). Reads were quality filtered using Trimmomatic (Bolger et al., 2014). Sequences were searched for all common Illumina adaptors and the settings used were: LEADING:10

606 TRAILING:10 SLIDINGWINDOW:5:15 MINLEN:50. mRNA abundance was calculated using
607 SalmonQuant with default settings and *Trypanosoma brucei* Lister strain 427 2018 v68
608 reference transcriptome and genomes from TriTrypDB (Aslett et al., 2010).
609
610 **Ligand uptake**
611 Bovine holo-transferrin (ThermoFisher) was dialyzed against PBS and labelled with Alexa
612 fluor 568 NHS ester (ThermoFisher) following the manufacturer's protocol. Canine
613 transferrin was obtained from Abbexa and loaded with iron using a four-fold molar excess of
614 ammonium iron (III) sulphate in presence of 5 mM sodium bicarbonate followed by dialysis
615 against 10 mM HEPES pH 7.4, 150 mM NaCl as described previously (Trevor et al.,
616 2019)(Trevor et al., 2019). Canine holo- transferrin was then labelled with Alexa fluor 568
617 NHS ester (ThermoFisher) as above. The Hp-Hb complex was purified as described (Lane-
618 Serff et al., 2014) and labelled with Alexa fluor 568 NHS ester (ThermoFisher) following the
619 manufacturer's protocol.
620
621 Mid log-phase cells (~ 6 x 10^5 /ml) were supplemented with 500 nM Alexa 568 labelled ligand
622 and incubated at 37°C. At time points, cells were fixed by the addition of 8% formaldehyde in
623 PBS to a final concentration 1% and incubated for 5 min. Cells were further washed with
624 PBS plus 1% BSA and DNA was stained with Hoechst 33258. Slides were prepared and
625 images were captured within next within the next 30 min using Zeiss Axio Imager.Z2 with
626 X100 objective. Samples in any one experiment were excited with the same intensity and
627 using the same exposure time. Images were processed using the ZEN Blue software.
628
629 **Immunofluorescence localisation and microscopy**
630 *T. brucei* cells were fixed in culture by the addition of one volume of 8% formaldehyde, 0.4%
631 glutaraldehyde (EM grade TAAB Laboratories Equipment Ltd.) in PBS for 10 min. After
632 fixation, cells were washed with serum free HMI-9 plus 1% bovine serum albumin (BSA)
633 twice and immobilized on poly-lysine coated slides for 1 hr. Immobilized cells were treated
634 with 0.1% triton X-100 (in PBS) for 5 min , washed with PBS and then incubated with PBS,
635 1% BSA for 10 min. Cells were incubated with the rabbit anti-TfR (1:50) or anti- FHR
636 (Macleod et al., 2020) (1:50) in PBS, 1% BSA for 1 hr, washed three times with PBS and
637 then with donkey anti- rabbit Alexa488 (1:800) in PBS, 1% BSA for 1 hr. Cells were washed
638 three times with PBS and the last wash contained 0.1 µg/ml Hoechst 33258 to stain DNA.
639 Cells were mounted with anti-fade and were visualized under Zeiss Axio Imager.Z2 with
640 X100 objective. In any one experiment, samples were illuminated with same exposure time,
641 intensity for respective excitation channels. All immunofluorescence experiments were
642 repeated three to six times with similar results. The images were processed with ZEN Blue

software by adjusting the brightness and contrast with the same changes being made to all images in any one experiment including the negative controls. Individual cells were manually outlined to define the whole-cell regions of interest (ROI), and background fluorescence was measured from cell-free regions within the same field using the ZEN Blue software and it was subtracted. For each condition, mean fluorescence intensity (arbitrary unit) was quantified from at least 50-100 cells across the repeated experiments. Mean fluorescence intensity was measured and background fluorescence intensity was subtracted. ImageJ software was used to measure the point fluorescence intensity of ligands and receptor antibodies by drawing a line perpendicular to the long axis of the cell, and the distribution profile against the distance was plotted. For 3D structured illumination, a Zeiss Elyra7 microscope with X63 objective was used in the Cambridge Advanced Imaging Centre. Slides were prepared as above and the processing of all images and the 3D reconstruction were performed with ZEN Blue software only by adjusting the brightness contrast. All raw and processed images are available at EMBL-EBI BioImage Archive accession S-BIAD2480.

659 **FIGURE LEGENDS**

660

661 **Figure 1. *T. brucei* transferrin receptor expressed from BES7 contains GPI-anchored**
662 **ESAG7.**

663 (A) Phylogenetic tree showing the relationship between ESAG6 and ESAG7 proteins from *T.*
664 *brucei* Lister 427 (Hertz-Fowler et al., 2008). The tree was assembled in Geneious Prime
665 (www.geneious.com) using an alignment by Muscle 5.1 followed by a neighbour joining tree
666 with 100 bootstraps and no outgroup on residues 1 to 332 of the alignment. BES7 ESAG 6.1
667 and 7 are shown in red.

668 (B) Variation in transferrin receptor expression in cell lines expressing VSGs from different
669 bloodstream form expression sites (BES). BES3-VSG118, BES1-VSG221, BES7-VSG224
670 cell lines are unmanipulated and the BES7-VSG221 was made after exchanging VSG224 for
671 VSG221 (see Figure 2A). Cell lysates were treated with PNGaseF and 2 x 10^6 cells
672 equivalents were loaded. Western blots were probed with anti-TfR, and then overprobed with
673 anti-VSG221. ESAG6 and ESAG7 plus GPI-anchor variants are indicated; BES3-VSG118
674 and BES1-VSG221 cell lysates contain ESAG7 without the GPI anchor. BES3-VSG118 and
675 BES7-VSG224 cell lysates did not show any VSG221. The presence of VSG221 protein
676 confirmed the switching of BES7 VSG224 to VSG221. Switching in VSG type did not affect
677 the expression pattern of native TfR (ESAG6/7 plus GPI) protein. Coomassie blue stained
678 SDS-PAGE gel to demonstrate loading of samples.

679

680 **Figure 2. The effect of BES identity and the number of GPI-anchors on the cellular TfR**
681 **levels.**

682 (A) Schematic illustrating the production of cell lines. For the addition and removal of ESAG7
683 GPI-anchor addition sequences, two constructs were used for each of BES1 and BES7. A
684 description of the construct is provided in the methods. For BES7, the same process was
685 used, one construct removing the GPI-anchor from ESAG7, the other leaving it intact. For
686 BES1, integration of one resulted in modification of ESAG7 to add a GPI-anchor, integration
687 of the second resulted in an unchanged ESAG7 polypeptide sequence. Restriction enzyme
688 sites used in cloning: P, PacI; E, EcoRI; S, SacI; Bs, BstEII and Bb, BsrBI. The VSG in
689 BES7-VSG224 cells was switched to VSG221 to remove any VSG-dependent variation. The
690 targeting construct conferred G418 resistance. (B) Transferrin receptor expression in the
691 following cell lines: BES7-VSG221 single (1-GPI) and double (2-GPI) GPI-anchored TfR and
692 BES1-VSG221 single and double GPI-anchored TfR. Cell lysates were treated with
693 PNGaseF and 2 x 10^6 cells equivalents were loaded per gel track. A western blot of the
694 samples was probed with anti-TfR then over probed with anti-VSG221 and anti-SCD6.
695 ESAG6 and ESAG7 plus GPI-anchor variants are indicated.

696 (C) TfR quantitation estimates from a minimum of three biological replicates of each cell line,
697 error bars display the standard deviation for each sample. Samples plus a dilution series
698 from BES7-221 were minimally separated by SDS-PAGE to compress TfR components to a
699 single band for analysis after western blotting, probed with anti-TfR and anti-SCD6. Donkey
700 anti-rabbit Alexa 488 was used as secondary antibody and band intensity was calculated by
701 ImageJ ensuring that signals taken for each reading were below saturation levels. Relative
702 quantitation was determined by mapping values to those obtained from a dilution series.
703 Measurements for SDC6 were used to normalise cell loading with the value for BES1-1GPI
704 anchor samples given an arbitrary value of 1. Statistical analysis was used a two-tailed
705 paired t-test, $**p \leq 0.01$; $*p \leq 0.05$.
706
707 **Figure 3. Transferrin endocytosis is rapid, in both single and double GPI-anchored**
708 **cells. Initial binding is to the cell surface and internalization is detected within 60 sec.**
709 Cultures of single (1-GPI) or double (2-GPI) GPI-anchored TfR expressing BES7-VSG221
710 and BES1-VSG221 cells were supplemented with 500 nM Alexa568 labelled holo- transferrin
711 (Tf_{A568}) and incubated for 15 sec, 60 sec or 600 sec and fixed by addition of formaldehyde for
712 5 min. Following washing with PBS containing 1% bovine serum albumin cells were
713 visualized under Zeiss Axio Imager.Z2 with X100 objective. Images in all these experimental
714 time points for both 1- and 2GPI TfR cells were captured with same intensity of excitation
715 and exposure time.
716 (A) Images showing the location of bound or endocytosed transferrin in representative cells
717 in populations and at time points as indicated. Scale bar is 5 µm. Images were processed
718 with ZEN Blue 3.4 software without any deconvolution. Larger numbers of cells are shown in
719 Supplementary Figure 3.
720 (B) The variation between individual cells in transferrin binding and uptake and endocytosis
721 shown by measurements of total fluorescence intensity of Tf_{A568} in BES7 VSG221 1- and 2-
722 GPI TfR cells at 15 sec, 60 sec and 600 sec. Measurements were obtained using Zen Blue
723 3.4 software and normalizing the background fluorescence (Table S2). Scatter plots of
724 measurements of individual cells are shown for 1-GPI (grey) and 2-GPI (purple) TfRs. The
725 average and standard deviation are shown for each cell line.
726 (C) Tf_{A568} fluorescence intensity distribution across transverse sections of randomly selected
727 cells was measured using ImageJ software. The plots are shown for both BES7 1- and 2-
728 GPI cell lines, showing the pattern of individual cells in different colours at 60 sec and 600
729 sec.
730 (D) (E) and (F) Same as (A) (B) and (C) but with BES1-VSG221 1- and 2GPI TfR expressing
731 cells and Table S3 corresponds to (E).
732

733 **Figure 4. Immunofluorescence localisation of single and double GPI-anchored**
734 **transferrin receptors to the entire plasma membrane.**
735 Cell lines expressing VSG221 and either 1- or 2-GPI TfR variants were fixed in culture with
736 final concentrations of 4% formaldehyde and 0.2% glutaraldehyde. Immunofluorescence
737 localisations were performed with rabbit anti-TfR followed by donkey anti-rabbit Alexa 488
738 (green). Cells were visualized using a Zeiss Axio Imager.Z2 with X100 objective. Images in
739 all these experimental sets were captured with same intensity of excitation and exposure
740 time.
741 (A) Localization in cell lines as indicated. Scale bar is 5 µm. Images were processed with
742 ZEN Blue 3.4 software. A larger number of cells is shown in Supp. Figure 5.
743 (B) Fluorescence distribution across transverse sections of the cells was measured using
744 ImageJ software. Plots are shown for both BES7-VSG221 TfR cell lines, each cell in a
745 different colour.
746 (C) Mean anti-TfR fluorescence intensity in individual cells of both BES1 VSG221 and BES7
747 VSG221 1- and 2-GPI TfR cell population was measured using ZEN Blue 3.4 and
748 normalized against the background fluorescence (Table S4). Bar diagram shows the
749 fluorescence intensity of either 1-GPI (grey) or 2-GPI (purple) TfR from individual cells. The
750 columns represent the average and the error bars show the standard deviation.
751
752 **Figure 5. Localization of single and double GPI-anchored transferrin receptors under**
753 **3D structured illumination microscope.**
754 Cells expressing either 1- or 2-GPI-anchored TfR were fixed in culture with final
755 concentrations of 4% formaldehyde and 0.2% glutaraldehyde. Immunofluorescence
756 localisation was performed with rabbit anti-TfR and donkey anti-rabbit Alexa 488. Cells were
757 visualized using a Zeiss Elyra7 microscope with X63 objective. Images in all these
758 experimental sets were captured with same intensity of excitation and exposure time. (A)
759 Localization of TfR in different cell lines as indicated. Scale bar is 5 µm.
760 (B) 3D projection generated using ZEN Blue 3.4 software example cells from the cell lines as
761 indicated. These images show the localization pattern of TfR on the cell surface as well as
762 within intracellular compartments. X-Y-Z axis is indicated. Scale bar 5 µm.
763
764 **Figure 6. Haptoglobin-haemoglobin endocytosis assay. Initial binding is to the cell**
765 **surface followed by rapid endocytosis.**
766 Cells were supplemented with 500 nM Alexa 568 labelled HpHb, incubated for 15 sec, 60
767 sec or 600 sec and fixed in culture with 1% formaldehyde. Following washing with PBS
768 containing 1% bovine serum albumin. Cells were visualized under Zeiss Axio Imager.Z2 with

769 x100 objective. Images in all these experimental time points were captured with same
770 excitation intensity and exposure time.
771 (A) Images showing the location of HpHb in +/+ and -/- cells at different time points in
772 representative cells as indicated. Images were processed with ZEN Blue 3.4 software. Scale
773 bar is 5 µm. A greater number of cells is shown in Supp. Figure 6.
774 (B) HpHb fluorescence intensity distribution over transverse section of cells at 15 sec
775 measured using ImageJ software. Individual cells are shown in different colours.
776
777 **Figure 7. The complement factor H receptor localises to the cell surface.**
778 The observation that abundant FHR expression occurred in cells grown in rabbit serum but
779 not in FBS supplemented medium was used to investigate its localisation.
780 (A) Western blot analysis of FHR expression in *T. brucei* EATRO1125 cells grown in medium
781 supplemented with either foetal bovine serum or rabbit serum. Cell lysates were not treated
782 with PNGaseF and $2x10^6$ cells equivalent were loaded. The blot was probed with rabbit anti-
783 FHR and then overprobed with anti-SCD6 for loading.
784 (B) Immunofluorescence determination of localisation of FHR in cell lines as indicated. Cells
785 were fixed in culture with final concentration of 4% formaldehyde and 0.2% glutaraldehyde.
786 Rabbit anti-FHR antibody was followed by donkey anti-rabbit Alexa 488 secondary antibody.
787 A set of cells grown in RbS, fixed similarly and stained only with secondary antibody was
788 used as a control for residual rabbit IgG from the growth medium and cells grown in FBS for
789 non-expressers. Cells were visualized using a Zeiss Axio Imager.Z2 with x100 objective.
790 Scale bar is 5 µm. A larger number of cells is shown in Supp. Figure 7
791 (C) Localisation of FHR by 3D structured illumination microscopy. Cells fixed as above were
792 visualised using a Zeiss Elyra7 with x63 objective. Images were processed with ZEN Blue
793 3.4 software. Two representative cells images showing FHR in white and merged panel with
794 DNA in blue. Scale bar is 5 µm.
795
796 **SUPPLEMENTARY FIGURE LEGENDS**
797
798 **Supp Figure 1. Relationship between ESAG7 variants.**
799 A. Clustal W alignment of the nucleotide sequences of ESAG7s showing the translation
800 termination codon in red. The sequence for GPI-addition is present in all genes but a series
801 of small deletions between nucleotides 980 and 1080 resulted in a frame shift and a new
802 stop codon that effectively removed the C-terminal ~50 residues from the open reading
803 frame.

804 B. Same alignment but just including ESAG7 from BES1 and BES7 showing the
805 conservation of the coding potential to the 3' side of the stop codon in BES1 ESAG7
806 indicating the shorter ESAG7 genes probably arose from a longer BES7-like variant.
807 Functional stop codons are in red.
808
809 **Supp Figure 2. Relationship between ESAG 6 and 7.**
810 Clustal W alignment of BES7 ESAG6 and 7 nascent polypeptide sequences. Predicted
811 processing sites are indicated by yellow highlighting. The N-terminal signal sequence
812 cleavage site was predicted using SignalP 6.0 and GPI-anchor addition sites by NetGPI 1.1
813 as detailed below the alignment.
814
815 **Supp Figure 3. Transferrin endocytosis is rapid, in both single and double GPI-**
816 **anchored cells. Initial binding is to the cell surface and internalization is detected**
817 **within 60 sec.**
818 Larger fields of cells from the experiments shown in Figure 3. Scale bar is 20 µm.
819
820 **Supp Figure 4. Controls for specificity of bovine transferrin binding to *T. brucei* BES7**
821 **VSG221 transferrin receptors.**
822 (A) Clustal W alignment of the polypeptide sequences of cow and dog transferrin.
823 (B) Cultures were supplemented with 500 nM Alexa568 labelled canine holo- transferrin and
824 incubated for 60 sec and fixed in culture by addition of formaldehyde to 1%. Following
825 washing with PBS containing 1% bovine serum albumin cells were visualized under Zeiss
826 Axio Imager.Z2 with x100 objective. Images for both BES7 VSG221 1- and 2-GPI TfR cells
827 were captured with same intensity of excitation and exposure time.
828 Images showing the absence of any bound or endocytosed canine transferrin in around forty
829 cells in population of both 1- and 2GPI TfR cells. Scale bar is 20 µm. Images were
830 processed ZEN Blue 3.4 software. (C) Cultures of single (1-GPI) GPI-anchored TfR
831 expressing BES7-VSG221 cells were supplemented with either 0.5 µM Tf_{A568} only, 2.5 µM
832 unlabelled Tf plus 0.5 µM Tf_{A568}, or 5 µM unlabelled Tf plus 0.5 µM Tf_{A568}, and incubated for
833 15 sec, then fixed by addition of formaldehyde for 5 min. DNA was stained with Hoechst.
834 Following washing with PBS containing 1% bovine serum albumin cells were visualized
835 under Zeiss Axio Imager.Z2 with X100 objective. Larger field views in all these experimental
836 sets were captured with same intensity of excitation and exposure time. (D) BES7 cells in
837 late logarithmic phase growth were counted by haemocytometer, harvested by centrifugation
838 and treated as follows: Left panel: Lane 1 (t=0 FBS): washed briefly in serum-free HMI-9 and
839 resuspended at 1 x 10^8 cells/ml in protein sample buffer; Lanes 2-5, washed briefly in serum-
840 free HMI-9 and resuspended at 1 x 10^6 cells/ml in HMI-9 + 10% FBS (Lanes 2 and 3) or

841 HMI-9 + 1% BSA (lanes 4 and 5) for a further 1 or 2 h prior to re-harvesting as described for
842 lane 1. Right hand panel contains half the samples used for the left side but treated with
843 PNGaseF prior to resuspension in protein sample buffer. 2 x 10^6 cells/lane were separated
844 by SDS-PAGE on 15% gels. Western blot analysis was performed with anti-TfR, anti-ISG65
845 and anti-SDC6 antibodies.
846
847 **Supp Figure 5. Immunofluorescence localisation of single and double GPI-anchored**
848 **transferrin receptors to the entire plasma membrane.**
849 (A) Different fixation protocols for the localisation of single GPI-anchored TfR expressed
850 from BES7. Cells were fixed in culture with final concentrations of either 4% formaldehyde
851 plus 0.2% glutaraldehyde, 4% formaldehyde, or washed with (1X PBS+ 1% BSA) then fixed
852 with 4% formaldehyde plus 0.2% glutaraldehyde. Immunofluorescence localisations were
853 performed with rabbit anti-TfR followed by donkey anti-rabbit Alexa 488 and DNA was
854 stained with Hoechst. A Zeiss Axio Imager.Z2 with X100 objective was used to visualise the
855 cells. Images in all these experimental sets were captured with same intensity of excitation
856 and exposure time. Scale bar is 5 µm. Images were processed with ZEN Blue 3.4 software.
857 (B) A larger number of cells is shown for Supp. Figure 5A. Scale bar is 20 µm.
858 (C) Larger fields of cells from the experiments shown in Figure 4. Scale bar is 20 µm.
859
860 **Supp Figure 6. Haptoglobin-haemoglobin endocytosis assay. Initial binding is to the**
861 **cell surface followed by rapid endocytosis.**
862 Larger fields of cells from the experiments shown in Figure 6. Scale bar is 20 µm.
863
864 **Supp Figure 7. The complement factor H receptor localises to the cell surface.**
865 Larger fields of cells from the experiments shown in Figure 7B. Scale bar is 20 µm.
866

867 **ACKNOWLEDGEMENTS**

868 We would like to thank: Luísa Figueiredo for the gift of the cell line expressing VSG224 from
869 BES7 and a BES7 TAR clone; Piet Borst for the transferrin receptor antibodies; Jay Bangs
870 for a lot of fun discussions (but no fish); and the Cambridge Advance Imaging Centre for
871 Super Resolution Microscopy.

872

873 **FUNDING**

874 MC and MH are Wellcome Investigators (MC, 217138/Z/19/Z; MH, 220797/Z/20/Z). Initial
875 funding for SB was from the Newton-Bhabha Fund.

References:

Afgan, E., Baker, D., Batut, B., van den Beek, M., Bouvier, D., Cech, M., Chilton, J., Clements, D., Coraor, N., Grüning, B. A., Guerler, A., Hillman-Jackson, J., Hiltemann, S., Jalili, V., Rasche, H., Soranzo, N., Goecks, J., Taylor, J., Nekrutenko, A., & Blankenberg, D. (2018). The Galaxy platform for accessible, reproducible and collaborative biomedical analyses: 2018 update. *Nucleic Acids Research*, *46*(W1), W537–W544. https://doi.org/10.1093/nar/gky379

Aslett, M., Aurrecoechea, C., Berriman, M., Brestelli, J., Brunk, B. P., Carrington, M., Depledge, D. P., Fischer, S., Gajria, B., Gao, X., Gardner, M. J., Gingle, A., Grant, G., Harb, O. S., Heiges, M., Hertz-Fowler, C., Houston, R., Innamorato, F., Iodice, J., … Wang, H. (2010). TriTrypDB: a functional genomic resource for the Trypanosomatidae. *Nucleic Acids Research*, *38*(Database issue), D457-62. https://doi.org/10.1093/nar/gkp851

Banerjee, S., Minshall, N., Webb, H., & Carrington, M. (2024). How are Trypanosoma brucei receptors protected from host antibody-mediated attack? *BioEssays : News and Reviews in Molecular, Cellular and Developmental Biology*, e2400053. https://doi.org/10.1002/bies.202400053

Bangs, J. D., Andrews, N. W., Hart, G. W., & Englund, P. T. (1986). Posttranslational modification and intracellular transport of a trypanosome variant surface glycoprotein. *The Journal of Cell Biology*, *103*(1), 255–263. https://doi.org/10.1083/jcb.103.1.255

Barcons-Simon, A., Carrington, M., & Siegel, T. N. (2023). Decoding the impact of nuclear organization on antigenic variation in parasites. *Nature Microbiology*, *8*(8), 1408–1418. https://doi.org/10.1038/s41564-023-01424-9

Beneke, T., Madden, R., Makin, L., Valli, J., Sunter, J., & Gluenz, E. (2017). A CRISPR Cas9 high-throughput genome editing toolkit for kinetoplastids. *Royal Society Open Science*, *4*(5), 170095. https://doi.org/10.1098/rsos.170095

Biebinger, S., Helfert, S., Steverding, D., Ansorge, I., & Clayton, C. (2003). Impaired dimerization and trafficking of ESAG6 lacking a glycosyl-phosphatidylinositol anchor. *Molecular and Biochemical Parasitology*, *132*(2), 93–96. https://doi.org/10.1016/j.molbiopara.2003.07.005

Billington, K., Halliday, C., Madden, R., Dyer, P., Barker, A. R., Moreira-Leite, F. F., Carrington, M., Vaughan, S., Hertz-Fowler, C., Dean, S., Sunter, J. D., Wheeler, R. J., & Gull, K. (2023). Genome-wide subcellular protein map for the flagellate parasite Trypanosoma brucei. *Nature Microbiology*, *8*(3), 533–547. https://doi.org/10.1038/s41564-022-01295-6

Bolger, A. M., Lohse, M., & Usadel, B. (2014). Trimmomatic: a flexible trimmer for Illumina sequence data. *Bioinformatics (Oxford, England)*, *30*(15), 2114–2120. https://doi.org/10.1093/bioinformatics/btu170

Bonhivers, M., Nowacki, S., Landrein, N., & Robinson, D. R. (2008). Biogenesis of the trypanosome endo-exocytotic organelle is cytoskeleton mediated. *PLoS Biology*, *6*(5), e105. https://doi.org/10.1371/journal.pbio.0060105

Chaudhri, M., Steverding, D., Kittelberger, D., Tjia, S., & Overath, P. (1994). Expression of a glycosylphosphatidylinositol-anchored Trypanosoma brucei transferrin-binding protein complex in insect cells. *Proceedings of the National Academy of Sciences of the United States of America*, *91*(14), 6443–6447. https://doi.org/10.1073/pnas.91.14.6443

Cook, A. D., Carrington, M., & Higgins, M. K. (2024). Molecular mechanism of complement inhibition by the trypanosome receptor ISG65. *ELife*, *12*. https://doi.org/10.7554/eLife.88960

Duncan, S. M., Carbajo, C. G., Nagar, R., Zhong, Q., Breen, C., Ferguson, M. A. J., & Tiengwe, C. (2024). Generation of a bloodstream form Trypanosoma brucei double glycosyltransferase null mutant competent in receptor-mediated endocytosis of transferrin. *PLoS Pathogens*, *20*(6), e1012333. https://doi.org/10.1371/journal.ppat.1012333

Engstler, M., Pfohl, T., Herminghaus, S., Boshart, M., Wiegertjes, G., Heddergott, N., & Overath, P. (2007). Hydrodynamic flow-mediated protein sorting on the cell surface of trypanosomes. *Cell*, *131*(3), 505–515. https://doi.org/10.1016/j.cell.2007.08.046

Engstler, M., Thilo, L., Weise, F., Grünfelder, C. G., Schwarz, H., Boshart, M., & Overath, P. (2004). Kinetics of endocytosis and recycling of the GPI-anchored variant surface glycoprotein in Trypanosoma brucei. *Journal of Cell Science*, *117*(Pt 7), 1105–1115. https://doi.org/10.1242/jcs.00938

Gadelha, C., Rothery, S., Morphew, M., McIntosh, J. R., Severs, N. J., & Gull, K. (2009). Membrane domains and flagellar pocket boundaries are influenced by the cytoskeleton in African trypanosomes. *Proceedings of the National Academy of Sciences of the United States of America*, *106*(41), 17425–17430. https://doi.org/10.1073/pnas.0909289106

Gadelha, C., Zhang, W., Chamberlain, J. W., Chait, B. T., Wickstead, B., & Field, M. C. (2015). Architecture of a Host-Parasite Interface: Complex Targeting Mechanisms Revealed Through Proteomics. *Molecular & Cellular Proteomics : MCP*, *14*(7), 1911–1926. https://doi.org/10.1074/mcp.M114.047647

Gerrits, H., Mussmann, R., Bitter, W., Kieft, R., & Borst, P. (2002). The physiological significance of transferrin receptor variations in Trypanosoma brucei. *Molecular and Biochemical Parasitology*, *119*(2), 237–247. https://doi.org/10.1016/s0166-6851(01)00417-0

Gilabert Carbajo, C., Cornell, L. J., Madbouly, Y., Lai, Z., Yates, P. A., Tinti, M., & Tiengwe, C. (2021). Novel aspects of iron homeostasis in pathogenic bloodstream form Trypanosoma brucei. *PLoS Pathogens*, *17*(6), e1009696. https://doi.org/10.1371/journal.ppat.1009696

Gíslason, M. H., Nielsen, H., Almagro Armenteros, J. J., & Johansen, A. R. (2021). Prediction of GPI-anchored proteins with pointer neural networks. *Current Research in Biotechnology*, *3*, 6–13. https://doi.org/10.1016/j.crbiot.2021.01.001

Hertz-Fowler, C., Figueiredo, L. M., Quail, M. A., Becker, M., Jackson, A., Bason, N., Brooks, K., Churcher, C., Fahkro, S., Goodhead, I., Heath, P., Kartvelishvili, M., Mungall, K., Harris, D., Hauser, H., Sanders, M., Saunders, D., Seeger, K., Sharp, S., … Berriman, M. (2008). Telomeric expression sites are highly conserved in Trypanosoma brucei. *PloS One*, *3*(10), e3527. https://doi.org/10.1371/journal.pone.0003527

962 Higgins, M. K., Tkachenko, O., Brown, A., Reed, J., Raper, J., & Carrington, M. (2013).
963 Structure of the trypanosome haptoglobin-hemoglobin receptor and implications for
964 nutrient uptake and innate immunity. *Proceedings of the National Academy of Sciences*
965 *of the United States of America*, *110*(5), 1905–1910.
966 https://doi.org/10.1073/pnas.1214943110

967 Hirumi, H., & Hirumi, K. (1989). Continuous cultivation of Trypanosoma brucei blood stream
968 forms in a medium containing a low concentration of serum protein without feeder cell
969 layers. *The Journal of Parasitology*, *75*(6), 985–989.

970 Hsia, R., Beals, T., & Boothroyd, J. C. (1996). Use of chimeric recombinant polypeptides to
971 analyse conformational, surface epitopes on trypanosome variant surface
972 glycoproteins. *Molecular Microbiology*, *19*(1), 53–63. https://doi.org/10.1046/j.1365-
973 2958.1996.351878.x

974 Kabiri, M., & Steverding, D. (2000). Studies on the recycling of the transferrin receptor in
975 Trypanosoma brucei using an inducible gene expression system. *European Journal of*
976 *Biochemistry*, *267*(11), 3309–3314. https://doi.org/10.1046/j.1432-1327.2000.01361.x

977 Kakuta, K., Orino, K., Yamamoto, S., & Watanabe, K. (1997). High levels of ferritin and its
978 iron in fetal bovine serum. *Comparative Biochemistry and Physiology. Part A,*
979 *Physiology*, *118*(1), 165–169. https://doi.org/10.1016/s0300-9629(96)00403-3

980 Lane-Serff, H., MacGregor, P., Lowe, E. D., Carrington, M., & Higgins, M. K. (2014).
981 Structural basis for ligand and innate immunity factor uptake by the trypanosome
982 haptoglobin-haemoglobin receptor. *ELife*, *3*, e05553.
983 https://doi.org/10.7554/eLife.05553

984 Lane-Serff, H., MacGregor, P., Peacock, L., Macleod, O. J., Kay, C., Gibson, W., Higgins, M.
985 K., & Carrington, M. (2016). Evolutionary diversification of the trypanosome
986 haptoglobin-haemoglobin receptor from an ancestral haemoglobin receptor. *ELife*, *5*.
987 https://doi.org/10.7554/eLife.13044

988 Leung, K. F., Riley, F. S., Carrington, M., & Field, M. C. (2011). Ubiquitylation and
989 developmental regulation of invariant surface protein expression in trypanosomes.
990 *Eukaryotic Cell*, *10*(7), 916–931. https://doi.org/10.1128/EC.05012-11

991 Ligtenberg, M. J., Bitter, W., Kieft, R., Steverding, D., Janssen, H., Calafat, J., & Borst, P.
992 (1994). Reconstitution of a surface transferrin binding complex in insect form
993 Trypanosoma brucei. *The EMBO Journal*, *13*(11), 2565–2573.
994 https://doi.org/10.1002/j.1460-2075.1994.tb06546.x

995 MacGregor, P., Gonzalez-Munoz, A. L., Jobe, F., Taylor, M. C., Rust, S., Sandercock, A. M.,
996 Macleod, O. J. S., Van Bocxlaer, K., Francisco, A. F., D'Hooge, F., Tiberghien, A., Barry,
997 C. S., Howard, P., Higgins, M. K., Vaughan, T. J., Minter, R., & Carrington, M. (2019). A
998 single dose of antibody-drug conjugate cures a stage 1 model of African
999 trypanosomiasis. *PLoS Neglected Tropical Diseases*, *13*(5), e0007373.
1000 https://doi.org/10.1371/journal.pntd.0007373

1001 Macleod, O. J. S., Bart, J.-M., MacGregor, P., Peacock, L., Savill, N. J., Hester, S., Ravel, S.,
1002 Sunter, J. D., Trevor, C., Rust, S., Vaughan, T. J., Minter, R., Mohammed, S., Gibson,
1003 W., Taylor, M. C., Higgins, M. K., & Carrington, M. (2020). A receptor for the
1004 complement regulator factor H increases transmission of trypanosomes to tsetse flies.
1005 *Nature Communications*, *11*(1), 1326. https://doi.org/10.1038/s41467-020-15125-y

1006 Macleod, O. J. S., Cook, A. D., Webb, H., Crow, M., Burns, R., Redpath, M., Seisenberger,
1007 S., Trevor, C. E., Peacock, L., Schwede, A., Kimblin, N., Francisco, A. F., Pepperl, J.,
1008 Rust, S., Voorheis, P., Gibson, W., Taylor, M. C., Higgins, M. K., & Carrington, M.
1009 (2022). Invariant surface glycoprotein 65 of Trypanosoma brucei is a complement C3
1010 receptor. *Nature Communications*, *13*(1), 5085. https://doi.org/10.1038/s41467-022-
1011 32728-9

1012 Maier, A., & Steverding, D. (2008). Expression and purification of non-glycosylated
1013 Trypanosoma brucei transferrin receptor in insect cells. *Experimental Parasitology*,
1014 *120*(2), 205–207. https://doi.org/10.1016/j.exppara.2008.07.004

1015 Mikkelsen, J. H., Stødkilde, K., Jensen, M. P., Hansen, A. G., Wu, Q., Lorentzen, J.,
1016 Graversen, J. H., Andersen, G. R., Fenton, R. A., Etzerodt, A., Thiel, S., & Andersen, C.
1017 B. F. (2024). Trypanosoma brucei Invariant Surface Glycoprotein 75 Is an
1018 Immunoglobulin Fc Receptor Inhibiting Complement Activation and Antibody-Mediated
1019 Cellular Phagocytosis. *Journal of Immunology (Baltimore, Md. : 1950)*, *212*(8), 1334–
1020 1344. https://doi.org/10.4049/jimmunol.2300862

1021 Mugnier, M. R., Cross, G. A. M., & Papavasiliou, F. N. (2015). The in vivo dynamics of
1022 antigenic variation in Trypanosoma brucei. *Science (New York, N.Y.)*, *347*(6229), 1470–
1023 1473. https://doi.org/10.1126/science.aaa4502

1024 Mussmann, R., Engstler, M., Gerrits, H., Kieft, R., Toaldo, C. B., Onderwater, J., Koerten, H.,
1025 van Luenen, H. G. A. M., & Borst, P. (2004). Factors affecting the level and localization
1026 of the transferrin receptor in Trypanosoma brucei. *The Journal of Biological Chemistry*,
1027 *279*(39), 40690–40698. https://doi.org/10.1074/jbc.M404697200

1028 Mussmann, R., Janssen, H., Calafat, J., Engstler, M., Ansorge, I., Clayton, C., & Borst, P.
1029 (2003). The expression level determines the surface distribution of the transferrin
1030 receptor in Trypanosoma brucei. *Molecular Microbiology*, *47*(1), 23–35.
1031 https://doi.org/10.1046/j.1365-2958.2003.03245.x

1032 Pays, E., Lips, S., Nolan, D., Vanhamme, L., & Pérez-Morga, D. (2001). The VSG
1033 expression sites of Trypanosoma brucei: multipurpose tools for the adaptation of the
1034 parasite to mammalian hosts. *Molecular and Biochemical Parasitology*, *114*(1), 1–16.
1035 https://doi.org/10.1016/s0166-6851(01)00242-0

1036 Pinger, J., Nešić, D., Ali, L., Aresta-Branco, F., Lilic, M., Chowdhury, S., Kim, H.-S., Verdi, J.,
1037 Raper, J., Ferguson, M. A. J., Papavasiliou, F. N., & Stebbins, C. E. (2018). African
1038 trypanosomes evade immune clearance by O-glycosylation of the VSG surface coat.
1039 *Nature Microbiology*, *3*(8), 932–938. https://doi.org/10.1038/s41564-018-0187-6

1040 Redpath, M. B., Windle, H., Nolan, D., Pays, E., Voorheis, H. P., & Carrington, M. (2000).
1041 ESAG11, a new VSG expression site-associated gene from Trypanosoma brucei.
1042 *Molecular and Biochemical Parasitology*, *111*(1), 223–228.
1043 https://doi.org/10.1016/s0166-6851(00)00305-4

1044 Roggy, J. L., & Bangs, J. D. (1999). Molecular cloning and biochemical characterization of a
1045 VCP homolog in African trypanosomes. *Molecular and Biochemical Parasitology*, *98*(1),
1046 1–15. https://doi.org/10.1016/s0166-6851(98)00114-5

1047 Salmon, D., Geuskens, M., Hanocq, F., Hanocq-Quertier, J., Nolan, D., Ruben, L., & Pays,
1048 E. (1994a). A novel heterodimeric transferrin receptor encoded by a pair of VSG
1049 expression site-associated genes in T. brucei. *Cell*, *78*(1), 75–86.
1050 https://doi.org/10.1016/0092-8674(94)90574-6

1051 Salmon, D., Geuskens, M., Hanocq, F., Hanocq-Quertier, J., Nolan, D., Ruben, L., & Pays,
1052 E. (1994b). A novel heterodimeric transferrin receptor encoded by a pair of VSG
1053 expression site-associated genes in T. brucei. *Cell*, *78*(1), 75–86.
1054 https://doi.org/10.1016/0092-8674(94)90574-6

1055 Schwartz, K. J., Peck, R. F., Tazeh, N. N., & Bangs, J. D. (2005). GPI valence and the fate of
1056 secretory membrane proteins in African trypanosomes. *Journal of Cell Science*, *118*(Pt
1057 23), 5499–5511. https://doi.org/10.1242/jcs.02667

1058 Schwede, A., Jones, N., Engstler, M., & Carrington, M. (2011). The VSG C-terminal domain
1059 is inaccessible to antibodies on live trypanosomes. *Molecular and Biochemical*
1060 *Parasitology*, *175*(2), 201–204. https://doi.org/10.1016/j.molbiopara.2010.11.004

1061 Steverding, D., Stierhof, Y. D., Chaudhri, M., Ligtenberg, M., Schell, D., Beck-Sickinger, A.
1062 G., & Overath, P. (1994a). ESAG 6 and 7 products of Trypanosoma brucei form a
1063 transferrin binding protein complex. *European Journal of Cell Biology*, *64*(1), 78–87.

1064 Steverding, D., Stierhof, Y. D., Chaudhri, M., Ligtenberg, M., Schell, D., Beck-Sickinger, A.
1065 G., & Overath, P. (1994b). ESAG 6 and 7 products of Trypanosoma brucei form a
1066 transferrin binding protein complex. *European Journal of Cell Biology*, *64*(1), 78–87.

1067 Steverding, D., Stierhof, Y. D., Fuchs, H., Tauber, R., & Overath, P. (1995). Transferrin-
1068 binding protein complex is the receptor for transferrin uptake in Trypanosoma brucei.
1069 *The Journal of Cell Biology*, *131*(5), 1173–1182. https://doi.org/10.1083/jcb.131.5.1173

1070 Tiengwe, C., Bush, P. J., & Bangs, J. D. (2017). Controlling transferrin receptor trafficking
1071 with GPI-valence in bloodstream stage African trypanosomes. *PLoS Pathogens*, *13*(5),
1072 e1006366. https://doi.org/10.1371/journal.ppat.1006366

1073 Trevor, C. E., Gonzalez-Munoz, A. L., Macleod, O. J. S., Woodcock, P. G., Rust, S.,
1074 Vaughan, T. J., Garman, E. F., Minter, R., Carrington, M., & Higgins, M. K. (2019).
1075 Structure of the trypanosome transferrin receptor reveals mechanisms of ligand
1076 recognition and immune evasion. *Nature Microbiology*, *4*(12), 2074–2081.
1077 https://doi.org/10.1038/s41564-019-0589-0

1078 van Luenen, H. G. A. M., Kieft, R., Mussmann, R., Engstler, M., ter Riet, B., & Borst, P.
1079 (2005). Trypanosomes change their transferrin receptor expression to allow effective
1080 uptake of host transferrin. *Molecular Microbiology*, *58*(1), 151–165.
1081 https://doi.org/10.1111/j.1365-2958.2005.04831.x

1082 Vanhollebeke, B., De Muylder, G., Nielsen, M. J., Pays, A., Tebabi, P., Dieu, M., Raes, M.,
1083 Moestrup, S. K., & Pays, E. (2008). A haptoglobin-hemoglobin receptor conveys innate
1084 immunity to Trypanosoma brucei in humans. *Science (New York, N.Y.)*, *320*(5876),
1085 677–681. https://doi.org/10.1126/science.1156296

1086 Ziegelbauer, K., Multhaup, G., & Overath, P. (1992). Molecular characterization of two
1087 invariant surface glycoproteins specific for the bloodstream stage of Trypanosoma
1088 brucei. *The Journal of Biological Chemistry*, *267*(15), 10797–10803.

1089 Ziegelbauer, K., & Overath, P. (1992). Identification of invariant surface glycoproteins in the
1090 bloodstream stage of Trypanosoma brucei. *The Journal of Biological Chemistry*,
1091 *267*(15), 10791–10796.

1092 Ziegelbauer, K., & Overath, P. (1993). Organization of two invariant surface glycoproteins in
1093 the surface coat of Trypanosoma brucei. *Infection and Immunity*, *61*(11), 4540–4545.
1094 https://doi.org/10.1128/iai.61.11.4540-4545.1993

1095

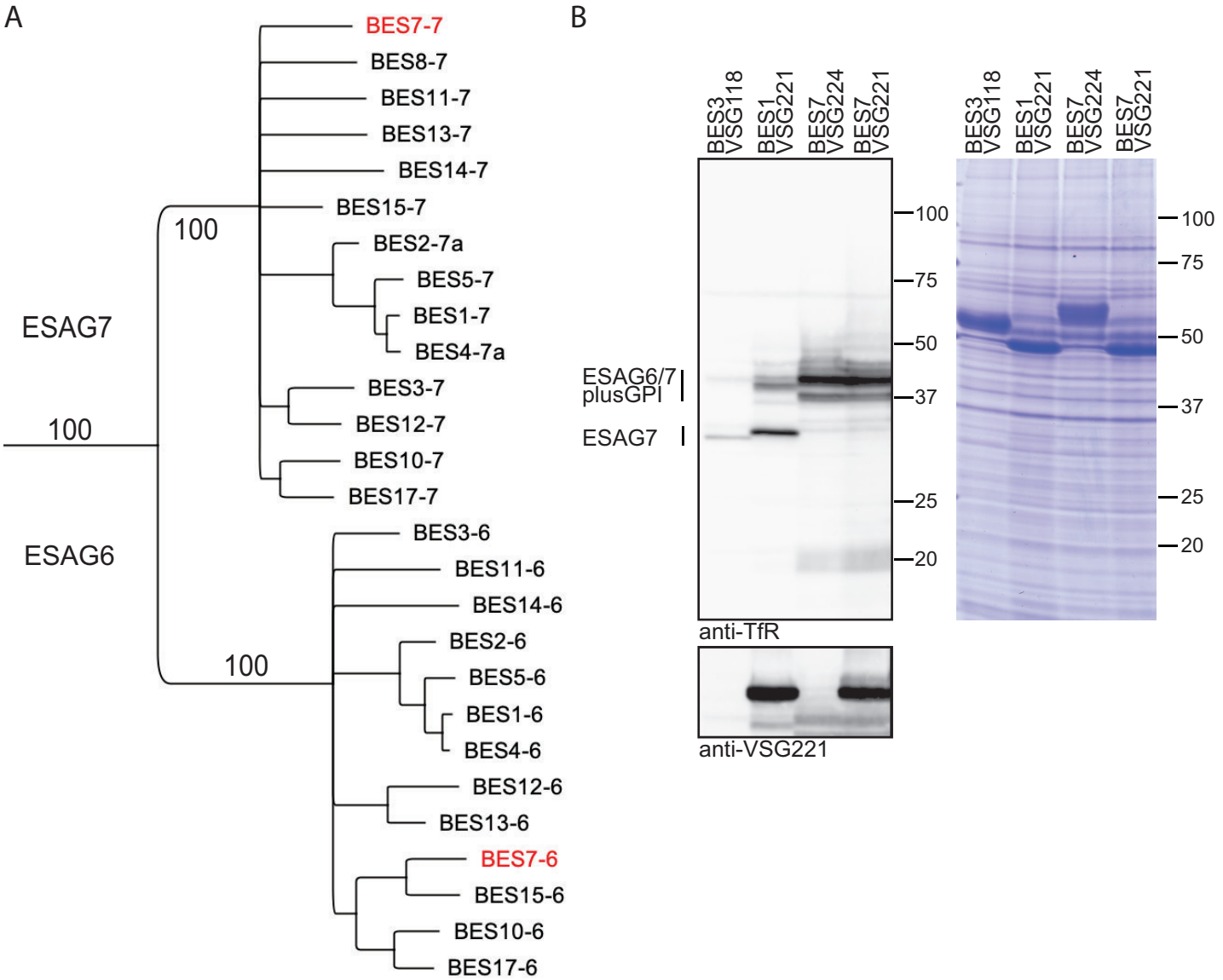
A
BES7-7
BES8-7
BES11-7
BES13-7
BES14-7
BES15-7
100
BES2-7a
BES5-7
BES1-7
BES4-7a
ESAG7
BES3-7
100
BES12-7
BES10-7
BES17-7
ESAG6
BES3-6
BES11-6
BES14-6
BES2-6
100
BES5-6
BES1-6
BES4-6
BES12-6
BES13-6
BES7-6
BES15-6
BES10-6
BES17-6
B
BES3 VSG118
BES1 VSG221
BES7 VSG224
BES7 VSG221
ESAG6/7 plusGPI
ESAG7
100
75
50
37
25
20
anti-TfR
anti-VSG221
BES3 VSG118
BES1 VSG221
BES7 VSG224
BES7 VSG221
100
75
50
37
25
20

Figure 1

A

Changes to BES7 ESAG7

altered anchor construct

ESAG6/7 genomic locus

unchanged anchor construct

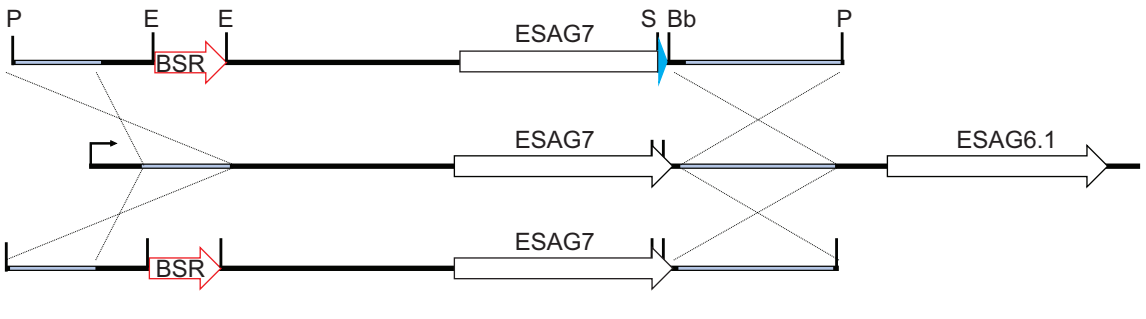

Changes to BES1 ESAG7

altered anchor construct

ESAG6/7 genomic locus

unchanged anchor construct

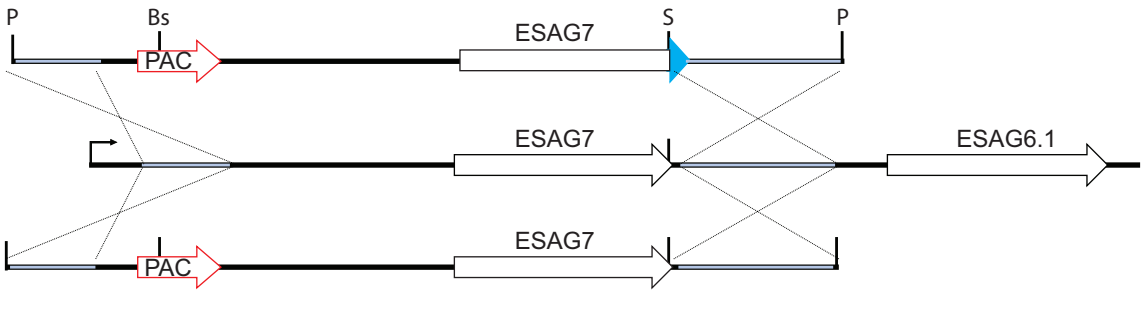

Changing BES7-VSG224 to BES7-VSG221

VSG224 genomic locus

replacement construct

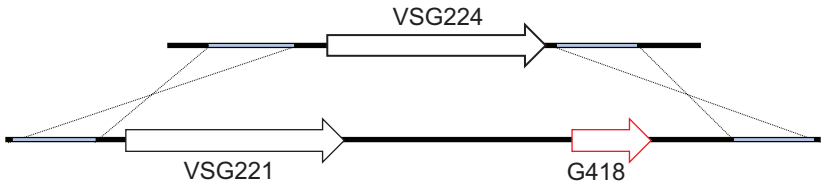

B

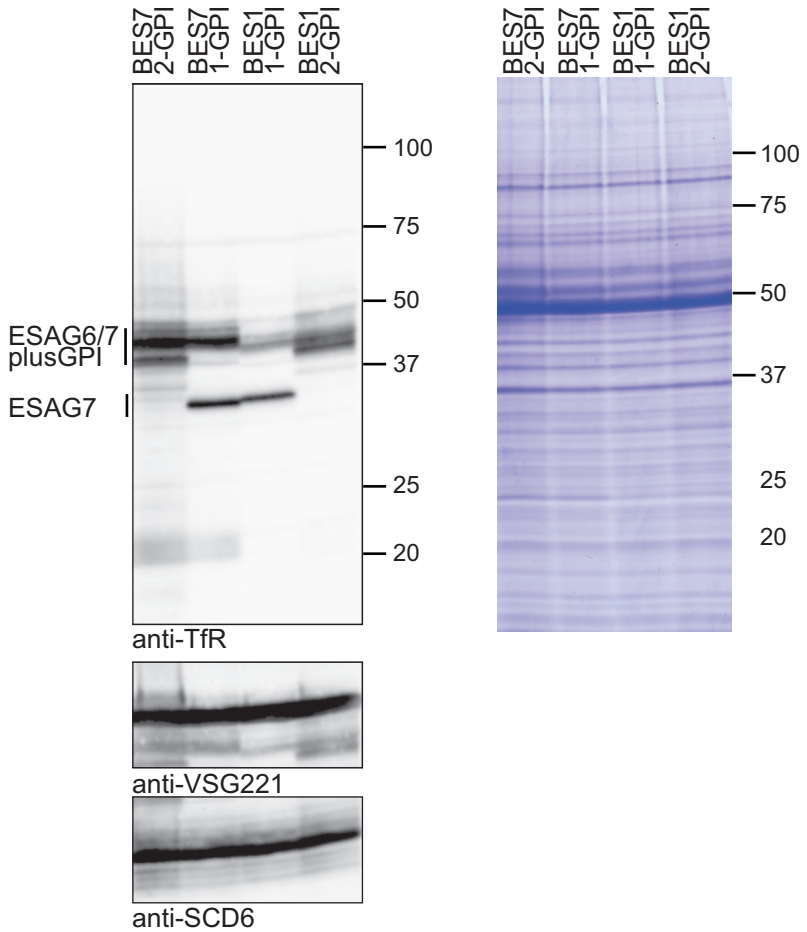

C

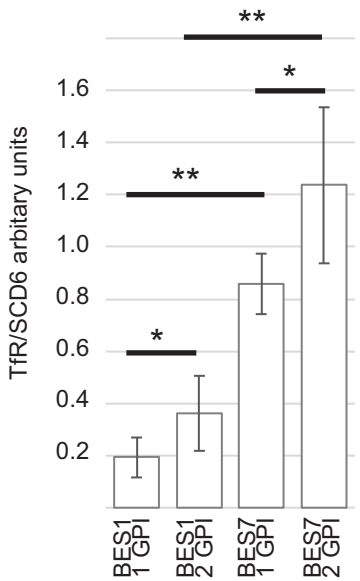

Figure 2

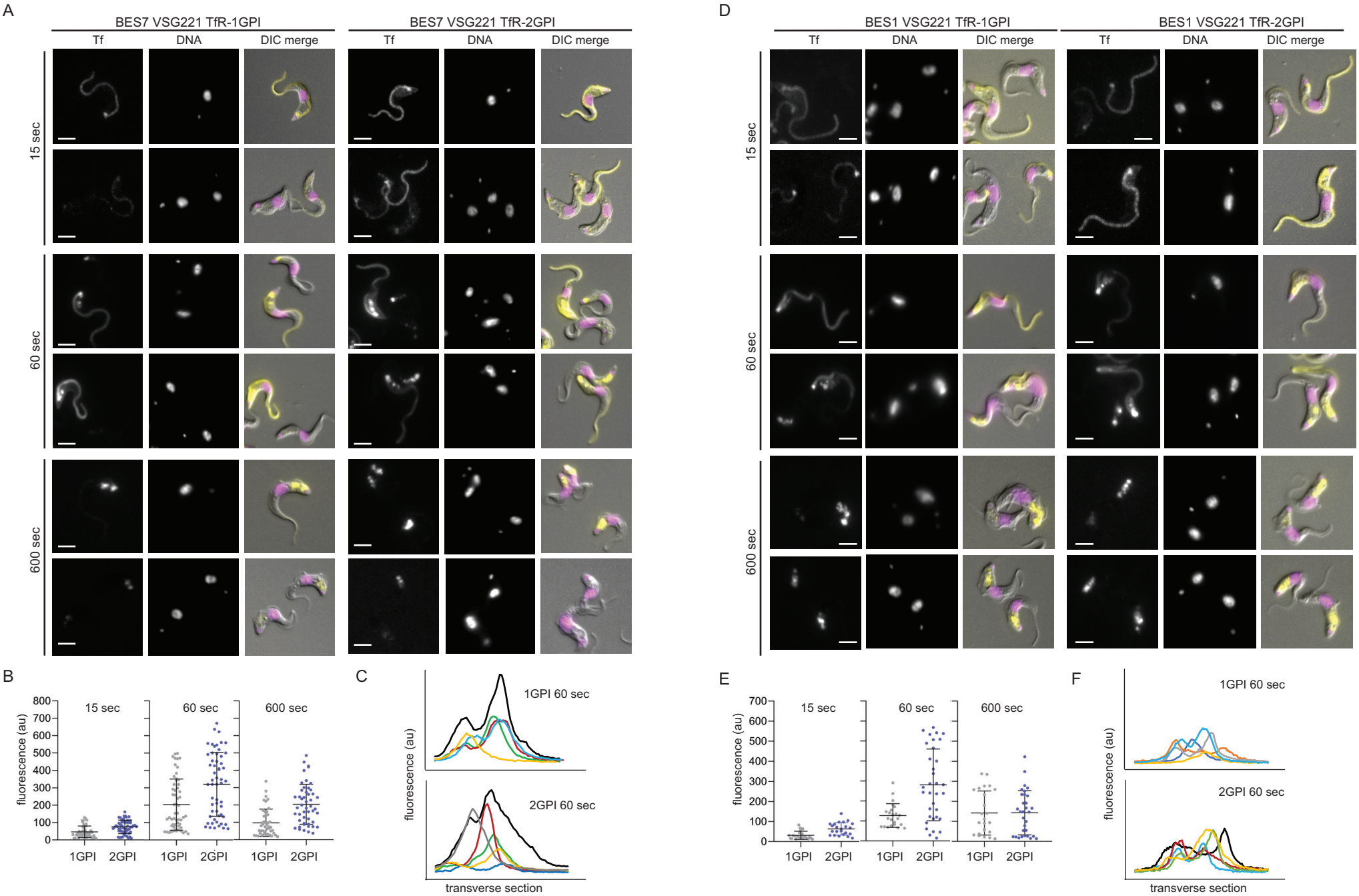
A
BES7 VSG221 TfR-1GPI
BES7 VSG221 TfR-2GPI
Tf
DNA
DIC merge
15 sec
60 sec
600 sec
D
BES1 VSG221 TfR-1GPI
BES1 VSG221 TfR-2GPI
B
fluorescence (au)
15 sec
60 sec
600 sec
1GPI
2GPI
C
1GPI 60 sec
2GPI 60 sec
transverse section
E
F

Figure 3

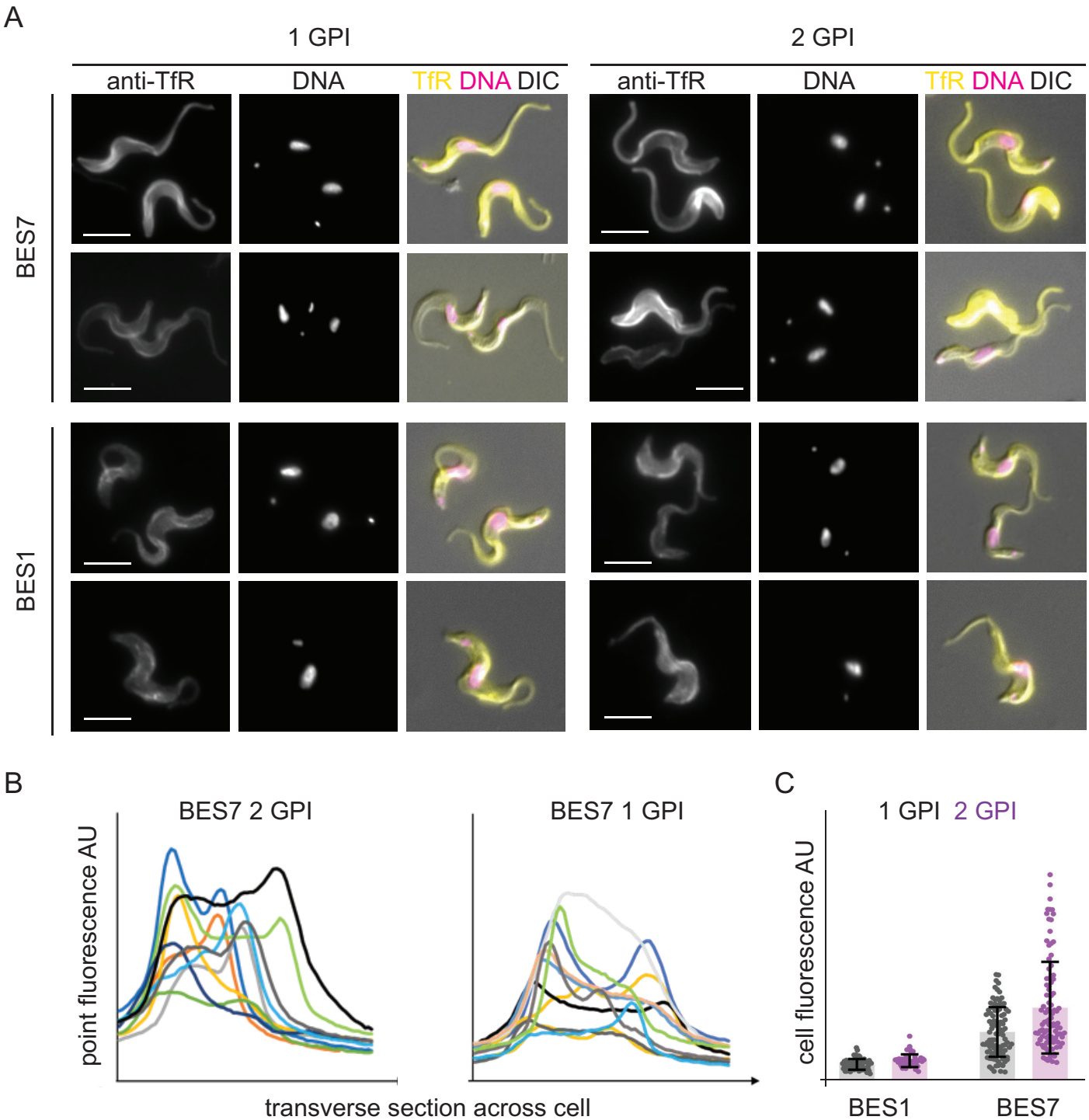
A
1 GPI
2 GPI
anti-TfR
DNA
TfR DNA DIC
anti-TfR
DNA
TfR DNA DIC
BES7
BES1
B
BES7 2 GPI
BES7 1 GPI
point fluorescence AU
transverse section across cell
C
1 GPI 2 GPI
cell fluorescence AU
BES1
BES7

Figure 4

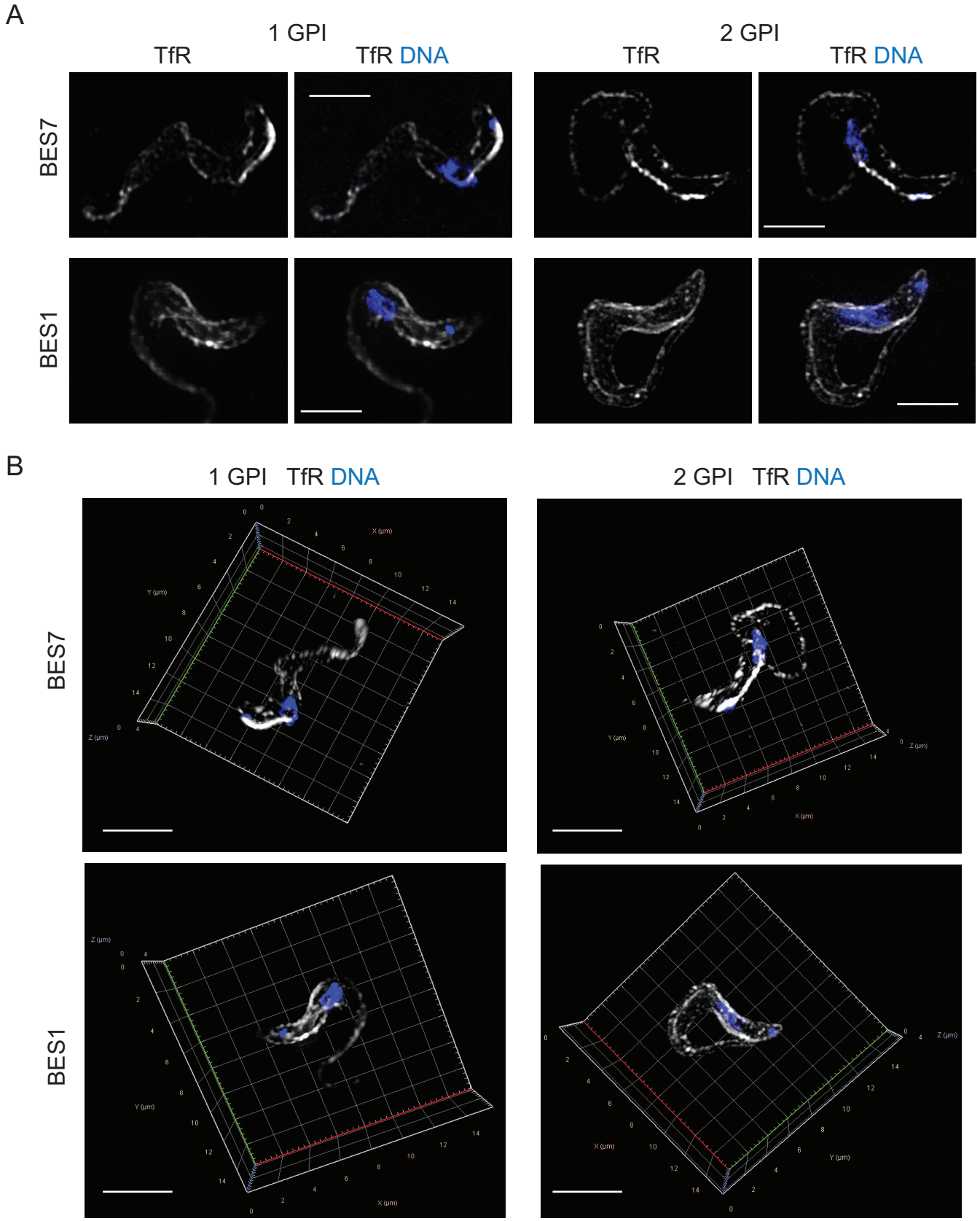
A
1 GPI
2 GPI
TfR
TfR DNA
TfR
TfR DNA
BES7
BES1
B
1 GPI TfR DNA
2 GPI TfR DNA
BES7
BES1

Figure 5

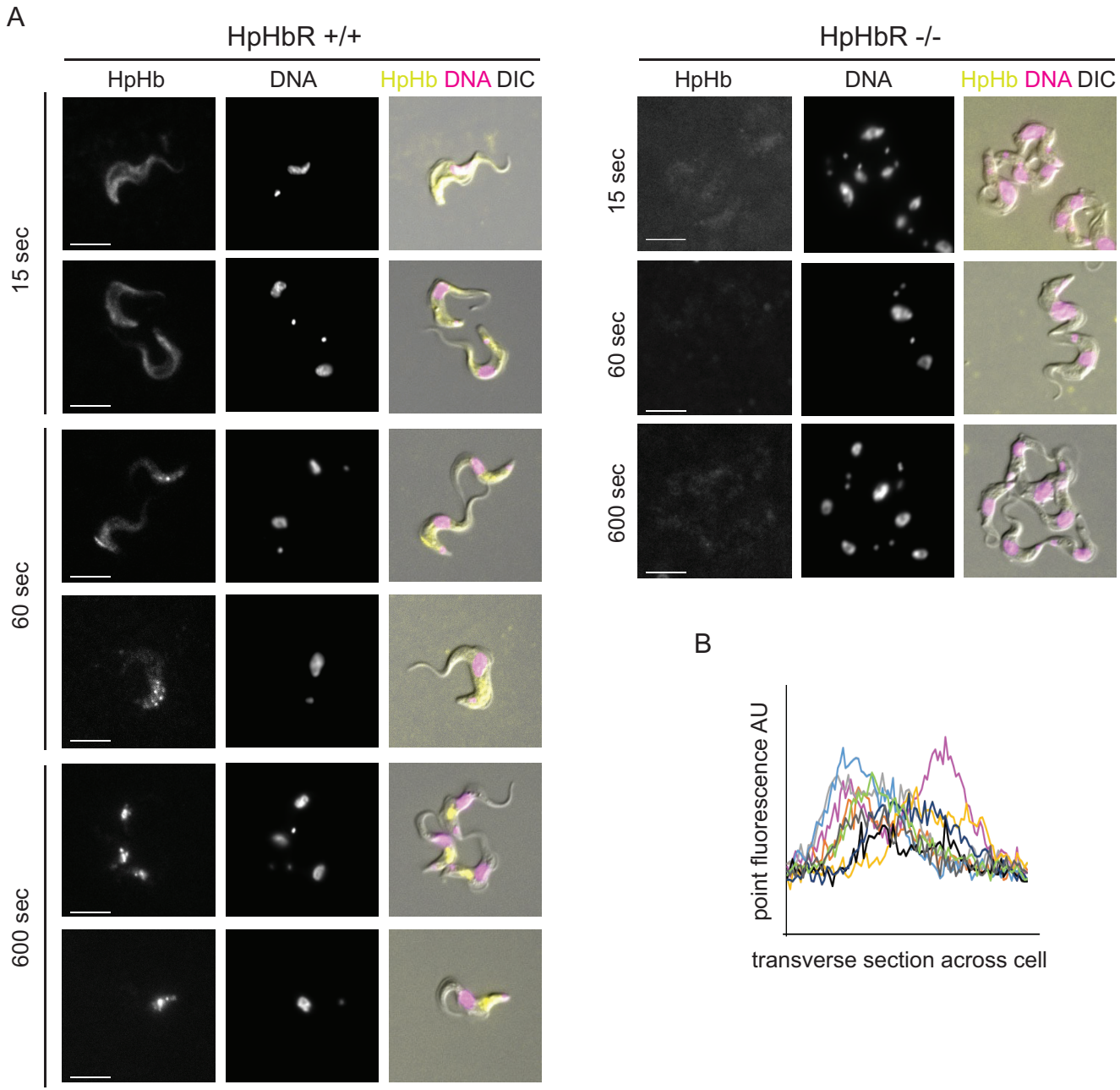
A
HpHbR +/+
HpHbR -/-
HpHb
DNA
HpHb DNA DIC
15 sec
60 sec
600 sec
B
point fluorescence AU
transverse section across cell

Figure 6

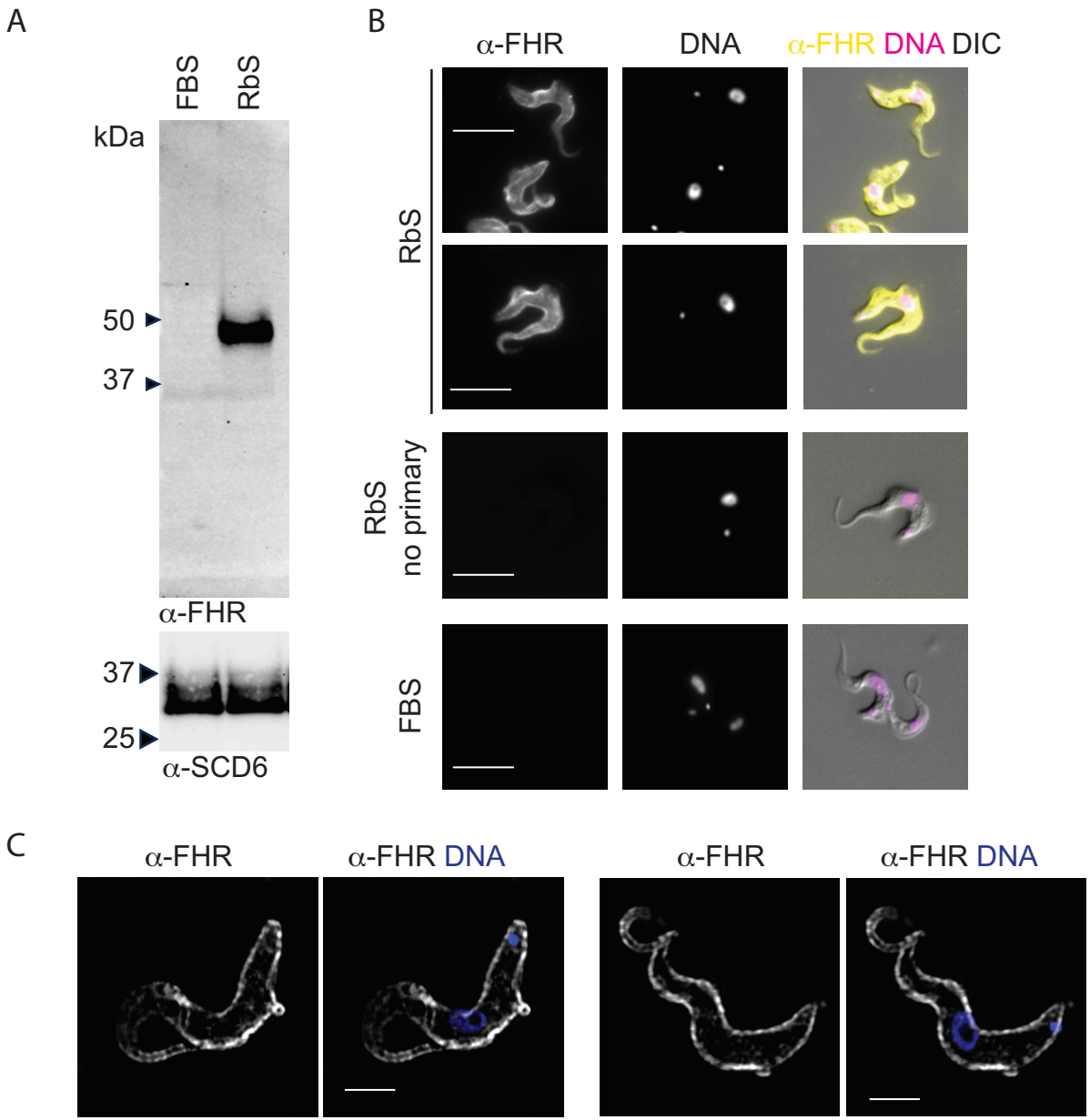
A
FBS
RbS
kDa
50
37
α-FHR
37
25
α-SCD6
B
α-FHR
DNA
α-FHR DNA DIC
RbS
RbS
no primary
FBS
C
α-FHR
α-FHR DNA
α-FHR
α-FHR DNA

Figure 7

A

ESAG7 ORFs from ~base 840

```
BES11    TTTAAGGATGTCATTCGCCTGTTTGCGCGCTTCAAAGAAGCAAAAAATGCAGTGATGAAGAAAATAAAAACTACTGTGGATGAATTGACTAAATGCATAGGGCAGAAAGAGGCTGAGCTC
BES2     TTTAAGGATGTCATCCGCCTGTTTGCGCGCTTCCAAGAAGCAAAAAATGCAGTGATGAATAAAATAAAAACTACTGTGGATGAATTGGCGAAATGCATAGGGCAGAAAGAGGTTGAGCTC
BES1     TTTAAGGATGTCATCCGCCTGTTTGCGCGCTTCCAAGAAGCAAAAAATGCAGTGATGAATAAAATAAAAACTACTGTGGATGAATTGGCGAAATGCATAGGGCAGAAAGAGGTTGAGCTC
BES4     TTTAAGGATGTCATTCGCCTGTTTGCGCGCTTCCAAGAAGCAAAAAATGCAGTGATGAATAAAATAAAAACTACTGTGGATGAATTGGCGAAATGCATAGGGCAGAAAGAGGTTGAGCTC
BES5     TTTAAGGATGTCATTCGCCTGTTTGCGCGCTTCCAAGAAGCAAAAAATGCAGTGATGAATAAAATAAAAACTACTGTGGATGAATTGGCGAAATGCATAGGGCAGAAAGAGGTTGAGCTC
BES7     TTTAAGGATGTCATTCGCCTGTTTGCGCGCTTCCAAGAAGCAAAAAATGCAGTGATGACGAAAATAAAAACTACTGTGGATGAATTGACGAAATGCATAGGGCAGAAGGAGGCTGAGCTC
BES13    TTTAAGGATGTCATTCGCCTGTTTGCGCGCTTCCAAGAAGCAAAAAATGCAGTGATGAGGAGAATAAAAACTACTGTGGATGAATTGACGAAATGTATAGGGAAGAAGGAGGCTGAACTC
BES14    TTTAAGGATGTCATTCGCCTGTTTGCGCGGTTCCAAGAAGCAAAAAATGAAGTGATGAATAAAATAAAAACTACTGTGGATGAATTGGCGAAATGCATAGGGCAGAAAGAGGTTGAGCTC
BES15    TTTAAGGATGTCATTCGCCTGTTTGCGCGGTTCCAAGAAGCAAAAAATGCAGTGATGACGAAAATAAAAACTACTGTGGATGAATTGACGAAATGCATAGGGCAGAAGGAGGCTGAACTC
BES12    TTTAAGGATGTCATTCGACTGTTTGCGCGCTTCCAAGAAGCAAAAAATGCAGTGATGAAGAAAATAAAAACTACTGTGGATGAATTGACGAAATGCATAGGGCAGAAAGAGGCTGAGCTC
BES3     TTTAAGGATGTCATTCGCCTGTTTGCGCGCTTCCAAGAAGTAAAAAATGCAGTGATGAAGAAAATAAAAACTACTGTGGATGAATTGACGAAATGCATAGGGCAGAAAGAGGCTGAGCTC
BES10    TTTAAGGATGTCATTCGCCTGTTTGCGCGCTTCCAAGAAGCAAAAAATGCAGTGATGAAGAAAATAAAAACTACTGTGGATGAATTGACGAAATGCATAGGGCAGAAGGAGGCTGAACTC
BES17    TTTAAGGATGTCATTCGCCTGTTTGCGCGCTTCCAAGAAGTAAAAAATGCAGTGGTGAAGAAAATAAAAACTACTGTGGATGAATTGACGAAATGCATAGGGCAGAAAGAGGCTGAGCTC
         ************** ** *********** *** ****** ******** **** ***  * ************************* * ***** ****** **** **** *** ***

BES11    ACTAATGATCAGCTTTACGAGGAATTT------GAGGCAATA----------------CAAAAGTATCTAGG-----------TTTTGGTAAAATGGAGTAAAAGC-----AAATTCAAC
BES2     ACTAATGATCAGCTTTACGAGGAATTC------GAGGCAATA----------------CAAAAGTACCTAGGG----------TCTCTGTGAAATGGAGTAAAAGC-----GAATTCAAC
BES1     ACTAATGATCAGCTTTACGAAGAATTC------GAGGCAATA----------------CAAAAGTACCTAGGG----------TCTCTGTGAAATGGAGTAAAGGC-----GAATTCAAC
BES4     ACTAATGATCAGCTTTACGAGGAATTC------GAGGCAATA----------------CAAAAGTACCTAGGG----------TCTCTGTGAAATGGAGTAAAAGC-----GAATTCAAC
BES5     ACTAATGATCAGCTTTACGAGGAATTC------GAGGCAATA----------------CAAAAGTACCTAGGG----------TCTCTGTGAAATGGAGTAAAAGC-----TAATTCAAC
BES7     ACTAATGATCAGCTTTACGAGGAATTTATCTGGGAGACCATAAACAGATTGGAGCTGTCAAAGAGAGTGAGTGAACAACCCTCTTTAGGTGAAGAAGAGGAGACGATCCTGAAATCTAAC
BES13    ACTAATGATCAGATTTACGAGGAATTC------GAGGCAATA----------------CAAAAGTATCTAGGG----------TTTCTGTGAAATGGAGTAAAAGC-----GAATCTAAC
BES14    ACTGATGATCAGCTTTACGAGGAATTC------GAGGCAATA----------------CAAAAGTATCTAGGG----------TTTCTGTGAAATGAAGTAAAAGC-----GAATCTAAC
BES15    ACTAATGATCAGATTTACGAGGAATTC------GAGGCAATA----------------CAAAAGTATCTAGGG----------TTTCTGTGAAATGGAGTAAAAGC-----GAATTTAAC
BES12    ACTAATGATCAGCTTTACGAGGAATTT------GAGGCAATA----------------CAAAAGTATCTAGGG----------TTTCTGTGAAATGGAGTAAAAGC-----GAATTTAAC
BES3     ACTAATGATCAGCTTTACGAGGAATTT------GAGGCAATA----------------CAAAAGTATCTATGG----------TTTCTGTGAAATGGAGTAAAAAC-----GAATCTAAC
BES10    ACTAATGATCAGATTTACGAGGAATTC------GAGGCAATA----------------CAAAAGTATCTAGGG----------TTTCTGTGAAATGGAGTAAAATC-----GAATCTAAC
BES17    ACTAATGATCAGCTTTACGAGGAATTT------GAGGTAATA----------------CAAAAGTATCTATGG----------TTTCTGTGAAATGGAGTAAAAAC-----GAATCTAAC
         *** ******** ******* *****       ***   ***                ****   *   *             * *  ** **    ** * *         ***  ***

BES11    TATACTGTAGAGCCTGTCTGGGGACCTTTCACGGGAGCGGGGTCCAACGCGGCAGCAATACATTCGAGTGTATCTACCGCTGCACTCTGTTGTTCAGTTTTATTGTTTGGAGTGCTGTGA
BES2     TATACTGCAGAACCGGTCCGGGGACATTTCACGGGAGCGGGGTCCAACGCGGCAGCAGTACATTTGAGTGTTTCTACCGCTGCACTTTGTTTTTCAGTTTTATTGTTGGGAGTGCTGTGA
BES1     TATACTGCAGAACCGGTCCGTGGACCTTTCACGGTAGCGGGGTCCAACACAGTAGCAGTACATTTGAGTGTTTCTACCGCTGCACTTTGTTTTTCAGTTTTATTGTTGGGAGTGCTGTGA
BES4     TATACTGCAGAACCGGTCCGGGGACATTTCACGGGAGCGGGGTCCAACGCGGCAGCAGTACATTTGAGTGTTTCTACCGCTGCACTTTGTTTTTCAGCTTTATTGTTGGGAGTGCTGTGA
BES5     TATACTGCAGAACCGGTCCGGGGACATTTCACGGGAGCGGGGTCCAACGCGGCAGCAGTACATTTGAGTGTTTCTACCGCTGCACTTTGTTTTTCAGCTTTATTGTTGGGAGTGCTGTGA
BES7     TATACTGCAGAACCTGTCCGTGGACCTTTCACGGGAGCGGGGGCCAACACAGTAGCAGTACAGTCGAGTGTTTCTACCGCTGCACTTTGTTGTTCAGCTTTATTGTTGGGAGTGCTGTGA
BES13    TATACTGTAGAACCTGTCCGTGGACCTTTCACGGGAGCGGGGTCCAACACAGTAGCAGTACATTTGAGTGTTTCTACCGCTGCACTCTGTTGTTTAGCTTTATTGTTGGGAGTGCTGTGA
BES14    TATACTGCAGAACCTGTCCGTGGACCTTTCACGGGAGCGGGGTCCAACACAGTAGCAGTACATTTGAGTGTTTCTACCGCTGCACTTTGTCGTTCAGCTTTATTGTTGGGAGTGCTGTGA
BES15    TATACTGCAGAACCTGTCCGTGGACCTTTCACGGGAGCGGGGTCCAACACAGTAGCAGTACAGTCGAGTGTTTCTACCGCTGCACTTTGTTGTTCAGTTTTATTGTTGGGAGTGCTGTGA
BES12    TATACTGCAGAACCTGTCCGTGGACCTTTCACTGGAGCGGGGGCCAATGCGGCAGCAATACATTTGAGTGTTTCTACCGCTGCACTTTGTTGTTCAGCTTTATTGTTGGGAGTGCTGTGA
BES3     TATACTGCAGAGCCTGTCCGTGGACCTTTAACGGGAGCGGGGGCCAACGCGGCAGCAATACATTTGAGTGTTTCTACCGCTGCACTTTGTCGTTCAGCTTTATTGTTGGGAGTGCTGTGA
BES10    TATACTGCAGAGCCTGTCCGTGGACCTTTAACGGGAGCGGGGGCCAACGCGGCAGCAATACATTTGAGTGTTTCTACCGCTGCACTTTGTCGTTCAGCTTTATTGTTGGGAGTGCTGTGA
BES17    TATACTGCAGAGCCTGTCCGTGGACCTTTCACGGTAGCGGGGGCCAACGCGGCAGCAATACATTTGAGTGTTTCTACCGCTGCACTTTGTCGTTCAGCTTTATTGTTGGGAGTGCTGTGA
         ******* *** ** *** * **** *** ** * ******* ****  * * **** **** * ****** ************** ***  ** ** ********* ******** ***
```

B

Comparison of ESAG7 from BES1 and BES7

```
         F  K  D  V  I  R  L  F  A  R  F  Q  E  A  K  N  A  V  M  T  K  I  K  T  T  V  D  E  L  T  K  C  I  G  Q  K  E  A  E  L
BES7     TTTAAGGATGTCATTCGCCTGTTTGCGCGCTTCCAAGAAGCAAAAAATGCAGTGATGACGAAAATAAAAACTACTGTGGATGAATTGACGAAATGCATAGGGCAGAAGGAGGCTGAGCTC
BES1     TTTAAGGATGTCATCCGCCTGTTTGCGCGCTTCCAAGAAGCAAAAAATGCAGTGATGAATAAAATAAAAACTACTGTGGATGAATTGGCGAAATGCATAGGGCAGAAAGAGGTTGAGCTC
F1        F  K  D  V  I  R  L  F  A  R  F  Q  E  A  K  N  A  V  M  N  K  I  K  T  T  V  D  E  L  A  K  C  I  G  Q  K  E  V  E  L

         T  N  D  Q  L  Y  E  E  F  I  W  E  T  I  N  R  L  E  L  S  K  R  V  S  E  Q  P  S  L  G  E  E  E  E  T  I  L  K  S  N
BES7     ACTAATGATCAGCTTTACGAGGAATTTATCTGGGAGACCATAAACAGATTGGAGCTGTCAAAGAGAGTGAGTGAACAACCCTCTTTAGGTGAAGAAGAGGAGACGATCCTGAAATCTAAC
BES1     ACTAATGATCAGCTTTACGAAGAATTC------GAGGCAATA----------------CAAAAGTACCTAGGG--------TCTCTGTGAAATGGAGTAAAGGC------GAATTC-AAC
F1        T  N  D  Q  L  Y  E  E  F       E  A  I                 Q  K  Y  L  G         S  L  *                          N

         Y  T  A  E  P  V  R  G  P  F  T  G  A  G  A  N  T  V  A  V  Q  S  S  V  S  T  A  A  L  C  C  S  A  L  L  L  G  V  L  *
BES7     TATACTGCAGAACCTGTCCGTGGACCTTTCACGGGAGCGGGGGCCAACACAGTAGCAGTACAGTCGAGTGTTTCTACCGCTGCACTTTGTTGTTCAGCTTTATTGTTGGGAGTGCTGTGA
BES1     TATACTGCAGAACCGGTCCGTGGACCTTTCACGGTAGCGGGGTCCAACACAGTAGCAGTACATTTGAGTGTTTCTACCGCTGCACTTTGTTTTTCAGTTTTATTGTTGGGAGTGCTGTGA
F1        Y  T  A  E  P  V  R  G  P  F  T  V  A  G  S  N  T  V  A  V  H  L  S  V  S  T  A  A  L  C  F  S  V  L  L  L  G  V  L  *
```

Figure S1

```
BES7-6.      MMRFWFVLLALLGKETY--AYENERNALNATAANKVCGLSTYLKGIAHRVNSESAVVTEK     58
BES7-7       -MRFLFVLLALLGKETHANYYENERNALNATAANKVCALSTYLKGIAHRVNSESAVVTEK     59
              *** ***********:   *****************.**********************

BES7-6       LSDLKMRSIQLQLSVMRNRVPSGEKDCKDIRTLLKTVLRNEFTFQQELEEMRSASALAAA     118
BES7-7       LSDLKMRSIQLQLSIMRNRVPSGEKDCKDIRTLLKTVLRNEFTFQQELEEVRNASALAAA     119
             **************:************************************:*.*******

BES7-6       AAGLAAGRLEEWIFVFAQAADGSSQFCISVGKTIPAEHGDLQECFDGKIGPETLYKIEDS     178
BES7-7       AAGLAAGRLEEWIFVFAQAGGRSSQFCISTGKTGPAEYNNLQECFDGTIGPETLYKIEDS     179
             *******************.. *******.*** ***:.:*******.************

BES7-6.      RVKESAQKSLQLHEVLSSISFGSLGVKNIVEKGENRGCNLMRTADEGLLKDVC-LNRNFT     237
BES7-7       RVKESAKTRLLLHEVLSSISFSSLGAENIRGGNGKDGCNLVRTDNNGILKGGSPTRHNLT     239
             ******:. * **********.***.:**   . : ****:** ::*:**. .  .:*:*

BES7-6       WGGGVLNFGYCVAGNLKIKGGEYGDVSSYDAVRWTEDPSKVSIFKDVIRLFARFQEAKNA     297
BES7-7       WGGGVMNFGSYQNGSMYVEGGEYGDATEYGAVRWTEDPSKVSIFKDVIRLFARFQEAKNA     299
             *****:***    *.: ::******.:.*.******************************

BES7-6       VMTKIKTTVDELTKCIGQKEAELTNDQLYEEFIWETINRLELSKRVSEQPSLGEEEETIL     357
BES7-7       VMTKIKTTVDELTKCIGQKEAELTNDQLYEEFIWETINRLELSKRVSEQPSLGEEEETIL     359
             ************************************************************

BES7-6       KSNYTAEPVRGPFTGAGANTVAVQSSVSTAALCCSALLLGVL     399
BES7-7       KSNYTAEPVRGPFTGAGANTVAVQSSVSTAALCCSALLLGVL     401
             ******************************************


# NetGPI 1.1      Timestamp: 20240925160446
# ID  Seq-length  Pred. GPI-Anchored      Omega-site pos.   Likelihood  Amino-acid
Sequence    399        GPI-Anchored      372                   0.438          G

ESAG6
# SignalP-6.0     Organism: Eukarya Timestamp: 20250215202022
# ID  Prediction  OTHER SP(Sec/SPI) CS Position
Sequence    SP    0.000369    0.999614    CS pos: 17-18. Pr: 0.9774

ESAG7
# SignalP-6.0     Organism: Eukarya Timestamp: 20250215202326
# ID  Prediction  OTHER SP(Sec/SPI) CS Position
Sequence    SP    0.000332    0.999656    CS pos: 18-19. Pr: 0.9760
```

Figure S2

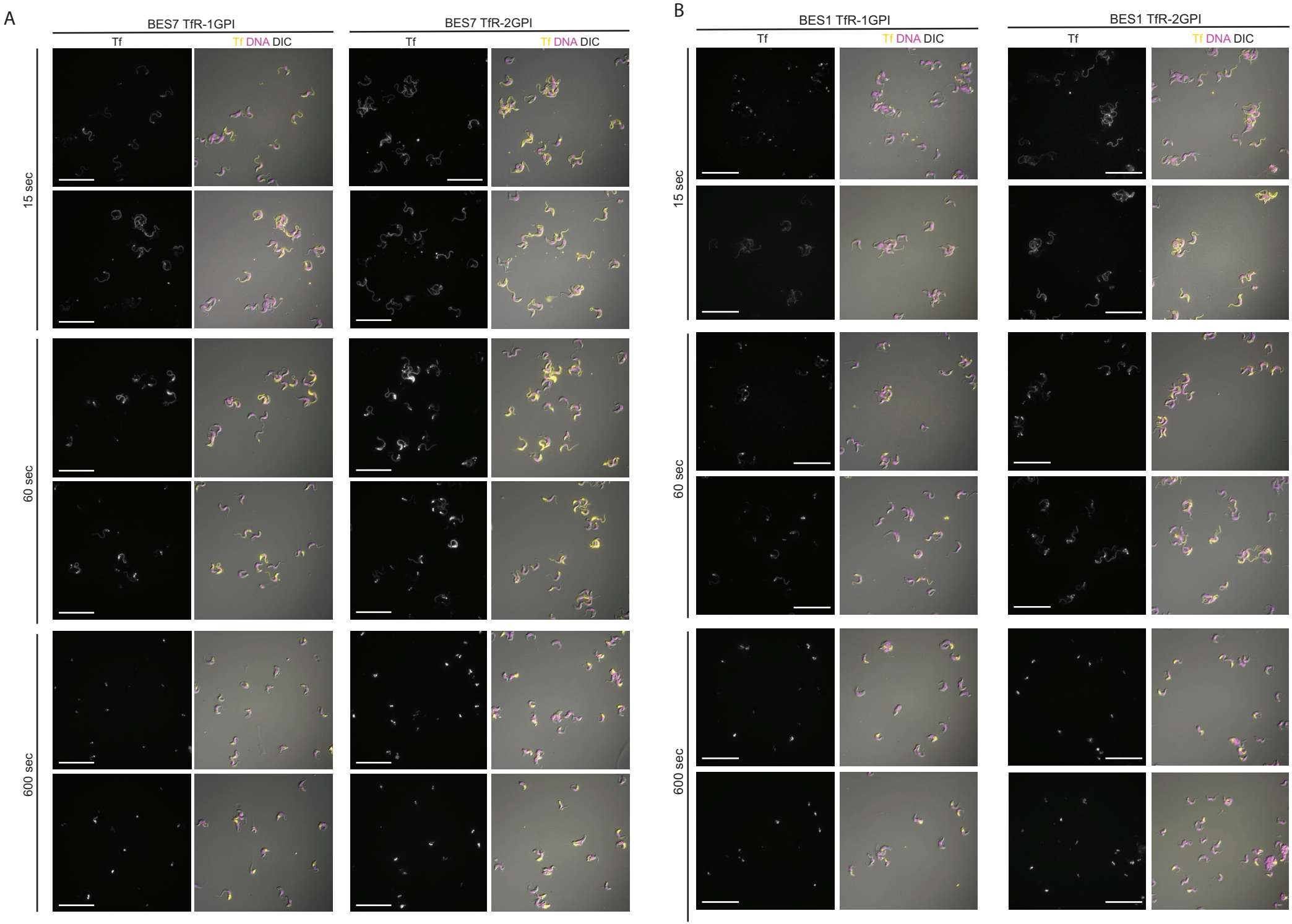
A
BES7 TfR-1GPI
BES7 TfR-2GPI
Tf
Tf DNA DIC
15 sec
60 sec
600 sec
B
BES1 TfR-1GPI
BES1 TfR-2GPI
Tf
Tf DNA DIC
15 sec
60 sec
600 sec

Figure S3

A

```
cow      -DPERTVRWCTISTHEANKCASFRENVLRILESGPFVSCVKKTSHMDCIKAISNNEADAV    59
dog      VSPEKTVRWCTVSNHEASKCSSFMENMKTVLENGPFVSCVKRTSYLECIKAIWANEADAV    60
          .**:******:*.***.**:** **:  :**.********:**:::*****  ******

cow      TLDGGLVYEAGLKPNNLKPVVAEFHGTKDNPQTHYYAVAVVKKDTDFKLNELRGKKSCHT    119
dog      TLDAGLVFEAGLNPYNLKPVVAEFYGKD--KQTRYYAVAVVKKSSTFNLNQLQGKKSCHT    118
         ***.***:****:* *********:*..   **:*********.: *:**:*:*******

cow      GLGRSAGWNIPMGKLYKELPDPQESIQRAAANFFSASCVPCADQSSFPKLCQLCAGKGTD    179
dog      GLGRSAGWNIPMGLLYWKLPEPRESLQKAASSFFTASCVPCVDRTAFPKLCQLCVGKGTD    178
         ************* ** :**:*:**:*:**:.**:******.*:::********.*****

cow      KCACSNHEPYFGYSGAFKCLMEGAGDVAFVKHSTVFDNLPNPEDRKNYELLCGDNTRKSV    239
dog      KCACSNHEPYFGYSGAFKCLMEDAGEVAFVKHSTVLENLPNKADLDQYELLCPDNKRKPV    238
         **********************.**:*********::****  * .:***** **.** *

cow      DNYQECYLAMVPSHAVVARTVGGKEDVIWELLNHAQEHFGKDKPDNFQLFQSPHGKDLLF    299
dog      GEYKQCYLAKVPSHAVVARSVGGKEDLIWELLNQAQEHYGKDKSKVFQLFSSTLGKDLLF    298
         .:*::**** *********:******:******:****:**** . ****.*  ******

cow      KDSADGFLKIPSKMDFELYLGYEYVTALQNLRESKPPDSSKDECM-VKWCAIGHQERTKC    358
dog      KDSAEGFFRIPPKMDTWLYLGYEYVTALRNLREDVRPDTPRDECKKVKWCAVGHHEIAKC    358
         ****:**::** ***  ***********:****.  **: :***  *****:**:* :**

cow      DRWSGFSGGAIECETAENTEECIAKIMKGEADAMSLDGGYLYIAGKCGLVPVLAENYKTE    418
dog      DEWSVNSEGKIECESAESTEDCIAKIAKGEADAMSLDGGYIYIAGQCGLVPVLAENYKTQ    418
         *.**  * * ****:**.**:***** *************:****:*************:

cow      DGSCKNTPEKGYLAVAVVKTSDANINWNNLKGKKSCHTAVDRTAGWNIPMGLLYSKINNC    478
dog      GSTCSNTAEEGYLAVAVVKELDKTISWNNLQGRKSCHTAVDRTAGWNIPMGLLYNRINHC    478
         ..:*.** *:*********  * .*.****:*:**********************.:**:*

cow      KFDEFFSAGCAPGSPRNSSLCALCIGSEKGTGKECVPNSNERYYGYTGAFRCLVEKGDVA    538
dog      EFDKFFSQGCAPGSMRNSSLCALCIGSANVPGKECVPNNHERYYGYTGAFRCLVEKGDVA    538
         :**:*** ****** ************ :  *******.:********************

cow      FVKDQTVIQNTDGNNNEAWAKNLKKENFEVLCKDGTRKPVTDAENCHLARGPNHAVVSRK    598
dog      FVKDQTVLQNTGGKNTEDWAKDLKEEDFELLCPDGQRKSVDKAPECFLAKAPNHAVVSRK    598
         *******:***.*:*.* ***:**:*:**:** ** ** * .* :*.**:.*********

cow      DKATCVEKILNKQQDDFGKSVTDCTSNFCLFQSNSKDLLFRDDTKCLASIAK-KTYDSYL    657
dog      DKASCVSKMLLDQQLLFGRNGNDCSGKFCLFHSATKDLLFRDDTQCLAKLPEDTTYKSYL    658
         ***:**.*:* .**  **:. .**:.:****:* :*********:***.: : .**.***

cow      GDDYVRAMTNLRQCSTSKLLEACTFHKP   685
dog      GAEYITAVANLRQCSTSKLLEACTFHTS   686
         * :*: *::*****************.

Identities
501/686
```

B

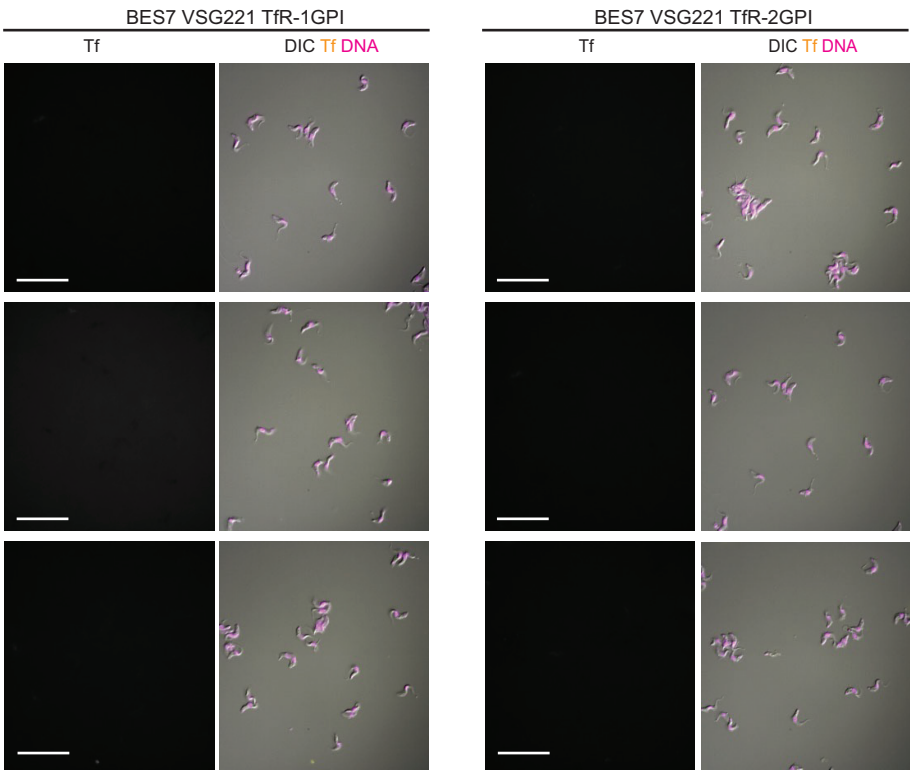

Figure S4

C

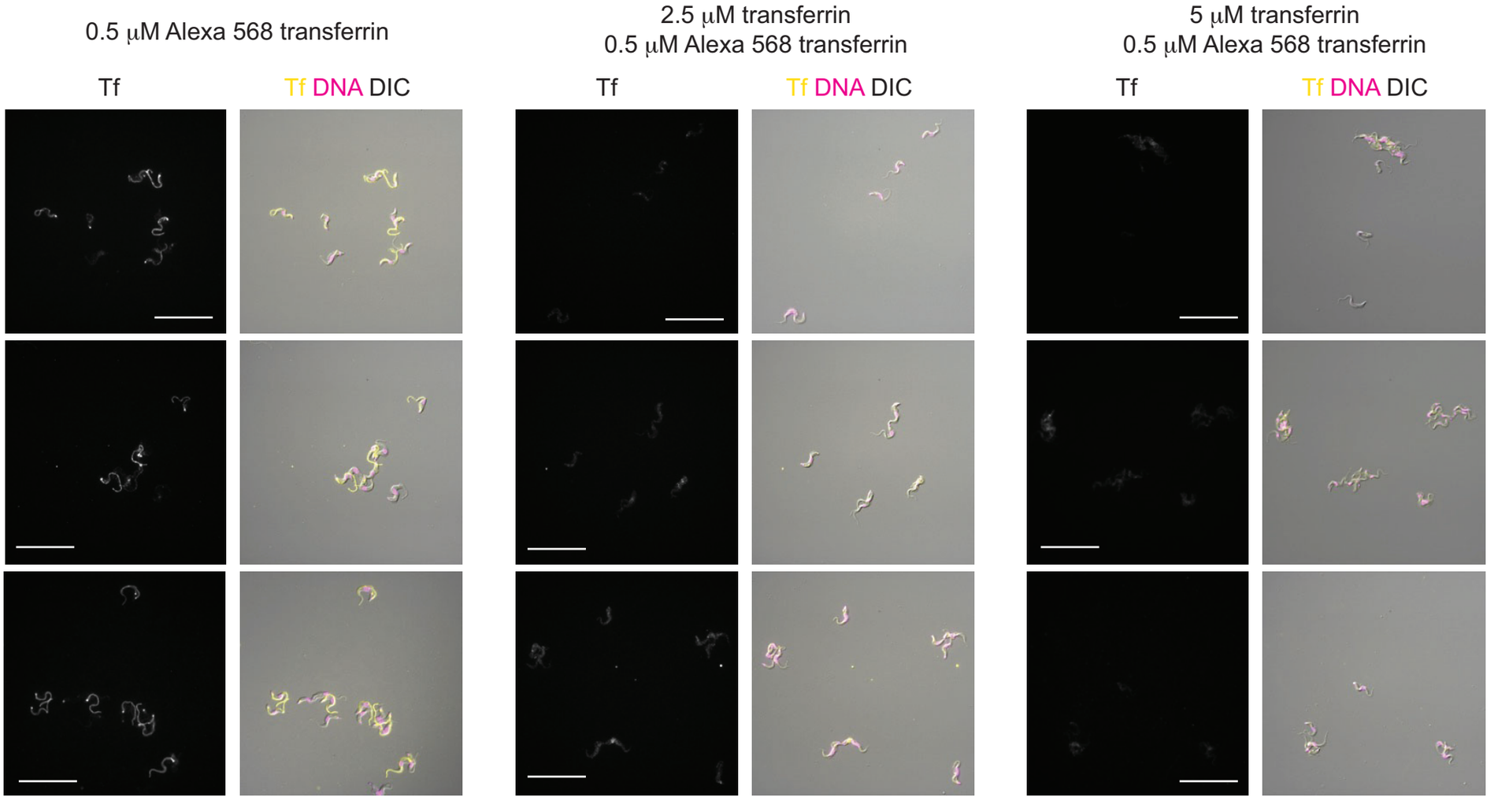
0.5 μM Alexa 568 transferrin
Tf
Tf DNA DIC
2.5 μM transferrin
0.5 μM Alexa 568 transferrin
Tf
Tf DNA DIC
5 μM transferrin
0.5 μM Alexa 568 transferrin
Tf
Tf DNA DIC

Figure S4

D

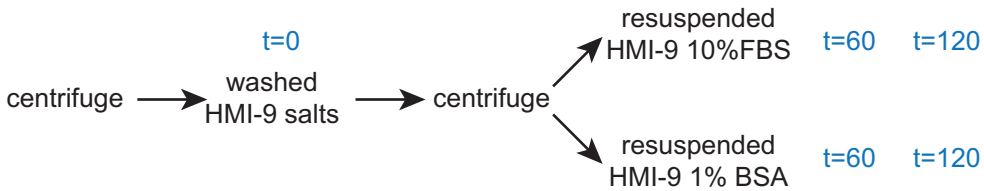
t=0
centrifuge
washed
HMI-9 salts
centrifuge
resuspended
HMI-9 10%FBS
t=60
t=120
resuspended
HMI-9 1% BSA
t=60
t=120

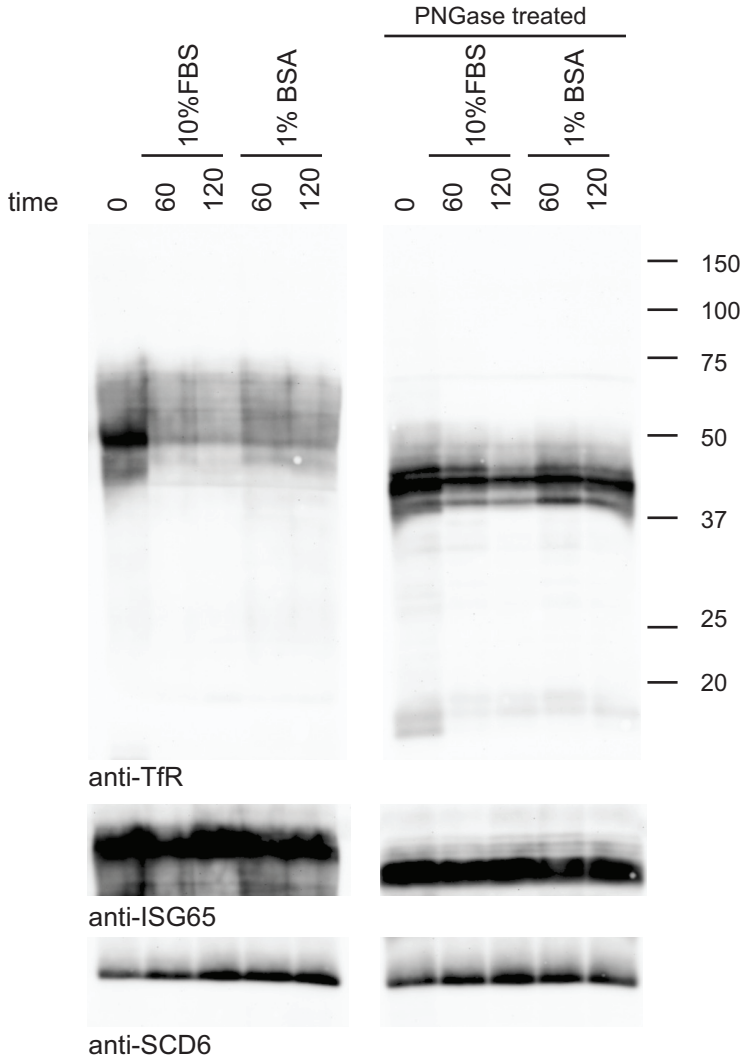
PNGase treated
10%FBS
1% BSA
10%FBS
1% BSA
time
0
60
120
60
120
0
60
120
60
120
150
100
75
50
37
25
20
anti-TfR
anti-ISG65
anti-SCD6

Figure S4

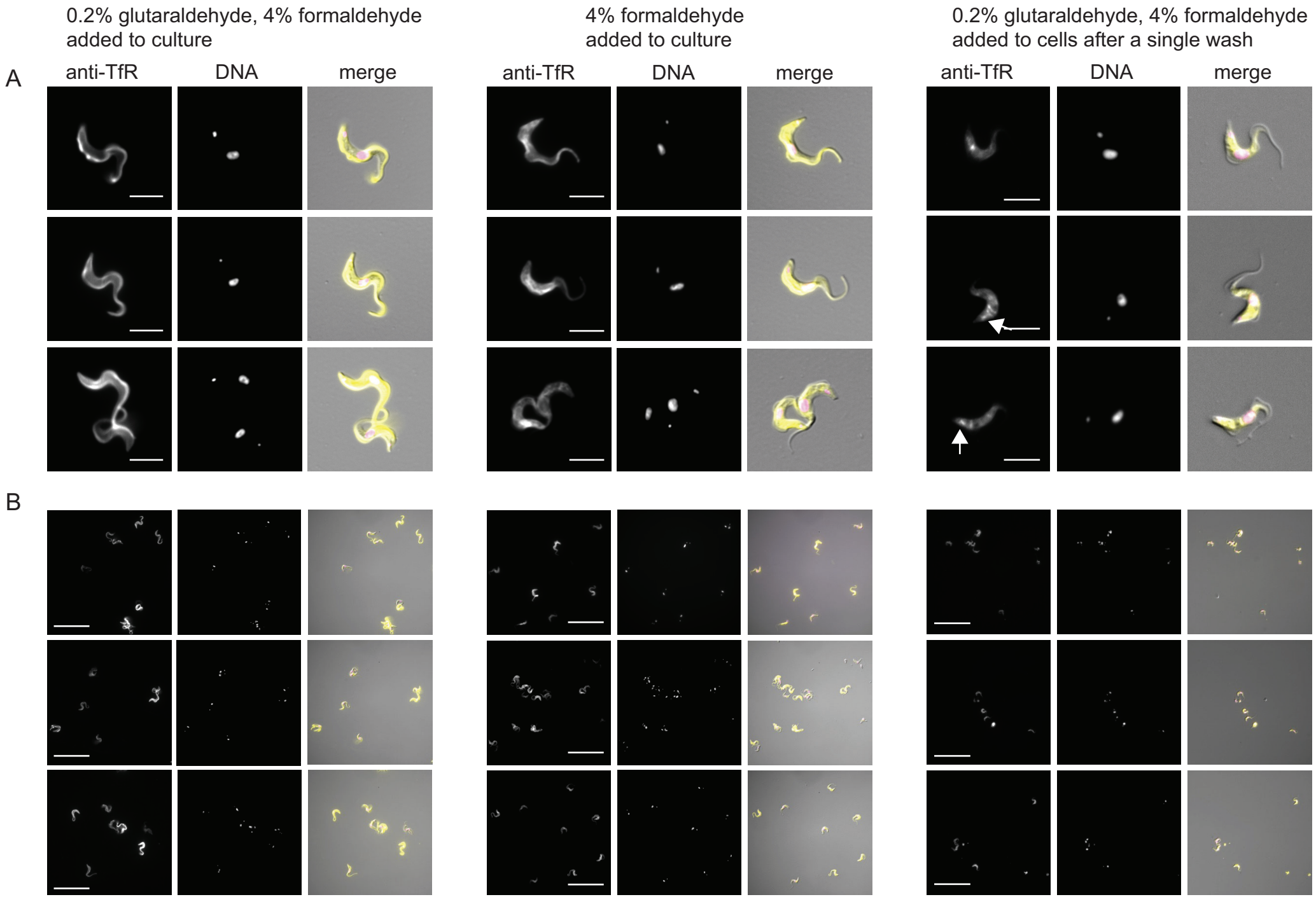
0.2% glutaraldehyde, 4% formaldehyde added to culture
4% formaldehyde added to culture
0.2% glutaraldehyde, 4% formaldehyde added to cells after a single wash
A
anti-TfR
DNA
merge
B

Figure S5

C

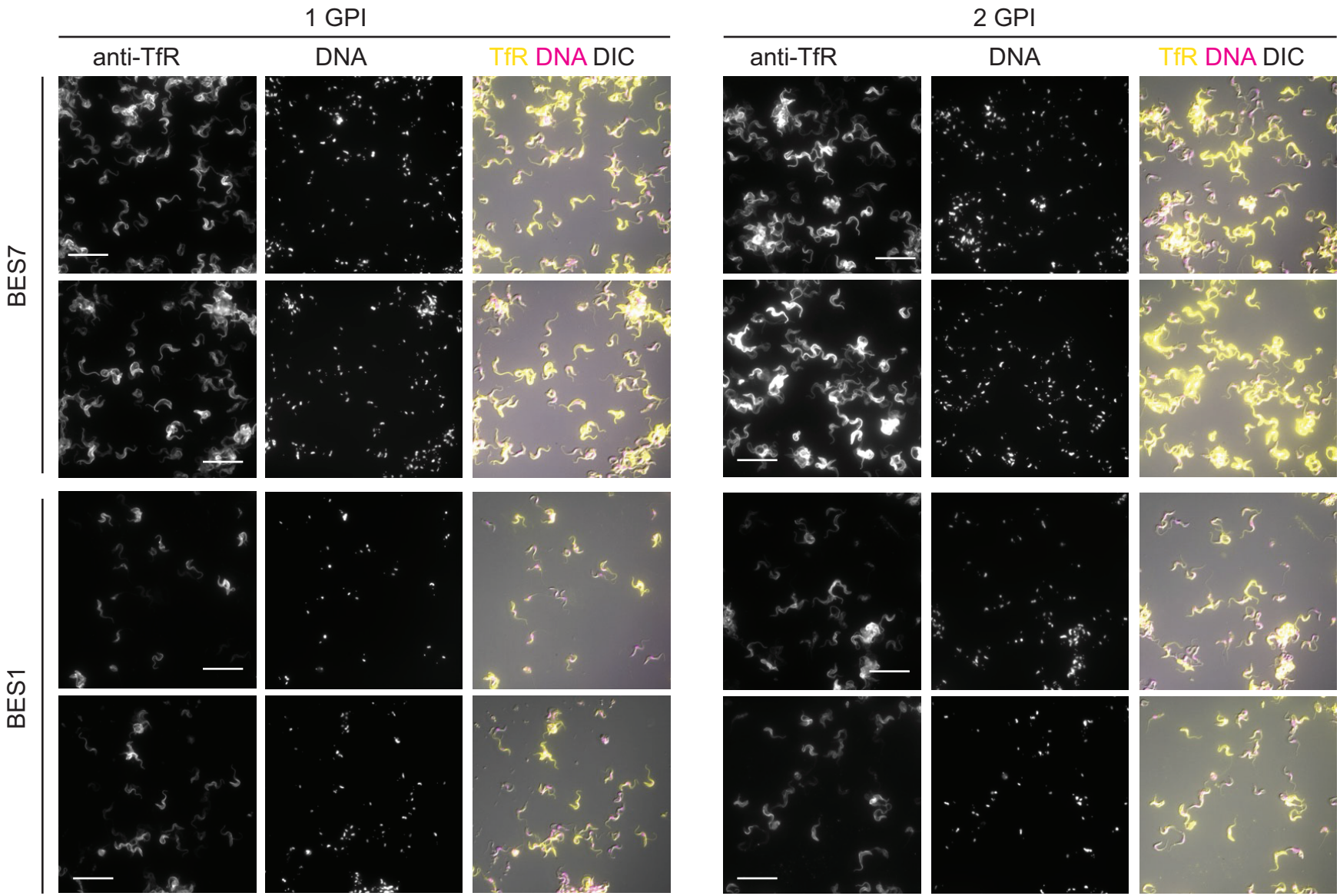
1 GPI
2 GPI
anti-TfR
DNA
TfR DNA DIC
anti-TfR
DNA
TfR DNA DIC
BES7
BES1

Figure S5

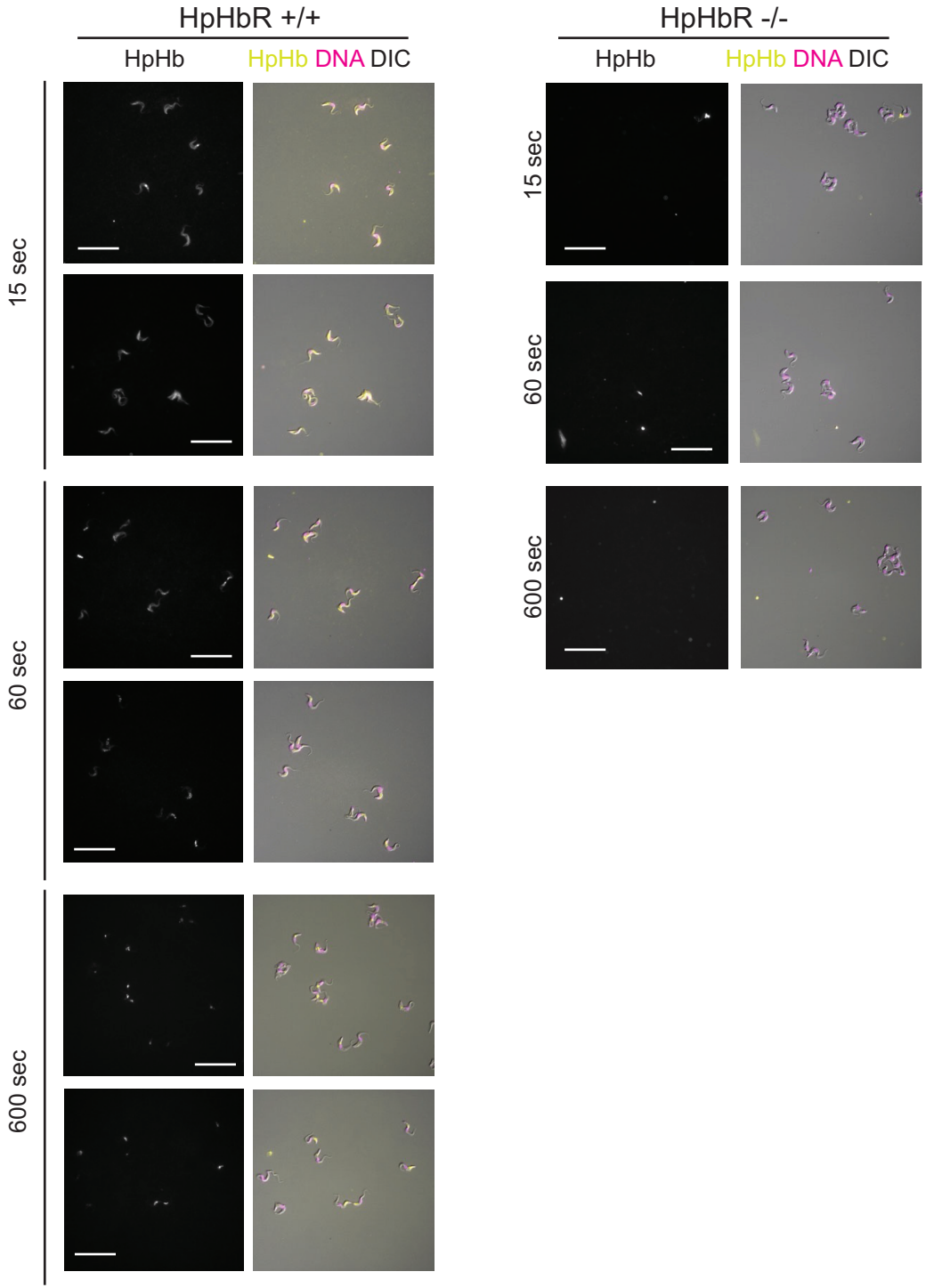
HpHbR +/+
HpHbR -/-
HpHb
HpHb DNA DIC
HpHb
HpHb DNA DIC
15 sec
60 sec
600 sec
15 sec
60 sec
600 sec

Figure S6

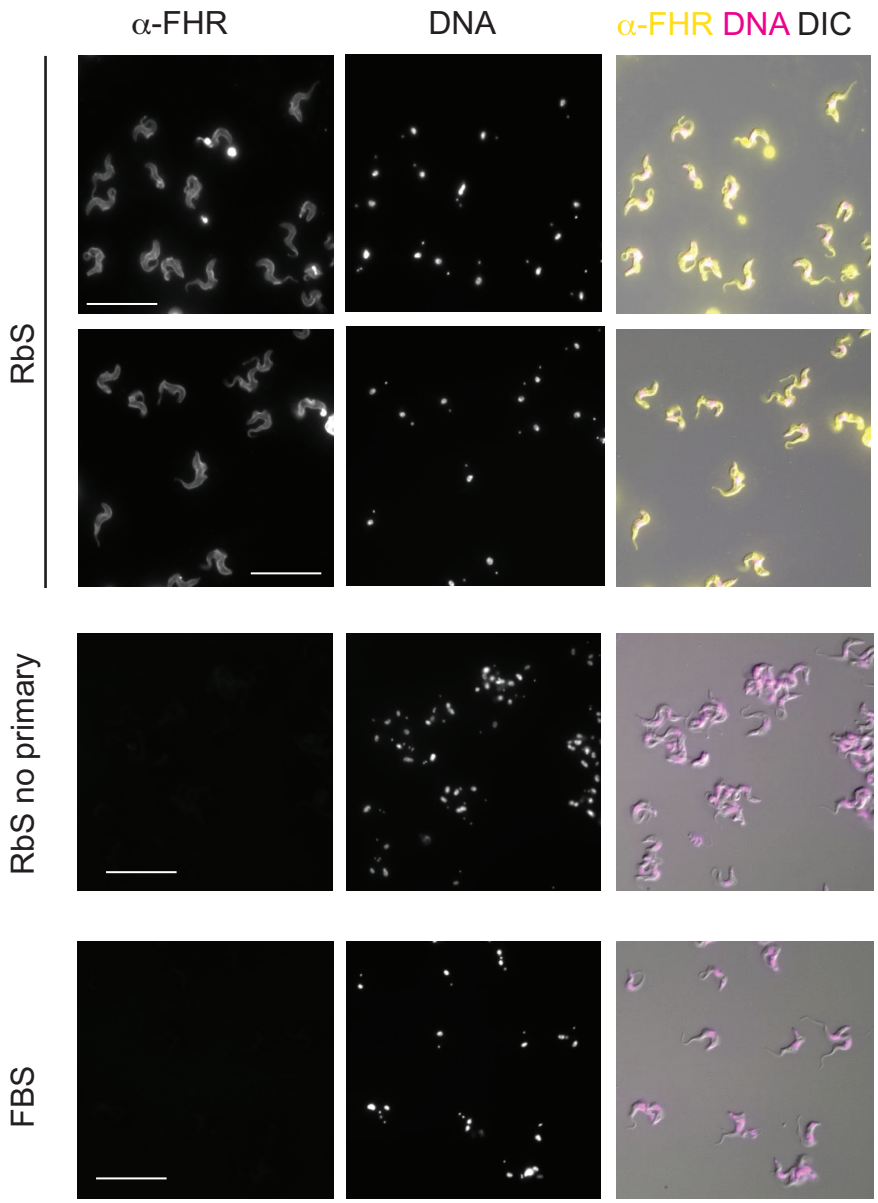

Figure S7

Table S1 VSG and TfR mRNA abundances in transcripts per million transcripts for BES3, BES1 and BES7 cell lines

Gene	BES3 TPM	BES1 TPM	BES7 TPM	Geneid
BES3 VSG	76528	13	0	Tb427_000487400
BES1 VSG	5	71558	9	Tb427_000016000
BES7 VSG	5	1	72659	Tb427_000025600
BES1 ESAG6	3	567	8	Tb427_000014400
BES1 ESAG7	4	893	15	Tb427_000014300
BES2 ESAG6	3	189	3	Tb427_000016400
BES2 ESAG7.1	3	149	4	Tb427_000016200
BES2 ESAG7.2	4	130	5	Tb427_000016300
BES3 ESAG6	420	9	14	Tb427_000019200
BES3 ESAG7	897	17	39	Tb427_000019100
BES4 ESAG6	5	127	4	Tb427_000020600
BES4 ESAG7.1	6	72	6	Tb427_000020400
BES4 ESAG7.2	6	70	6	Tb427_000020500
BES5 ESAG6	11	140	8	Tb427_000022500
BES5 ESAG7	8	50	7	Tb427_000022400
BES7 ESAG6.1	6	4	1129	Tb427_000024300
BES7 ESAG6.2	4	6	1568	Tb427_000024400
BES7 ESAG7	5	6	2076	Tb427_000024200
BES10 ESAG6	51	4	11	Tb427_000005600
BES10 ESAG7	44	8	31	Tb427_000005500
BES11 ESAG6	4	3	29	Tb427_000006100
BES11 ESAG7	5	4	10	Tb427_000006000
BES12 ESAG6	11	17	29	Tb427_000007400
BES12 ESAG7	16	12	41	Tb427_000007500
BES13 ESAG6	7	7	24	Tb427_000008500
BES13 ESAG7	7	6	16	Tb427_000008600
BES14 ESAG6	5	19	24	Tb427_000009700
BES14 ESAG7	10	20	62	Tb427_000009600
BES15 ESAG6	15	41	146	Tb427_000011200
BES15 ESAG7	48	89	198	Tb427_000011100
BES17 ESAG6	78	9	26	Tb427_000013100
BES17 ESAG7	32	15	60	Tb427_000013000
ESAG6	**622**	**1142**	**3024**	
ESAG7	**1096**	**1542**	**2573**	
ESAG 6+7 total	**1718**	**2683**	**5597**	
ESAG 6+7 total/VSG	**0.022**	**0.038**	**0.077**	

Table S2
BES7 1GPI

15sec			**60sec**			**600sec**		
Tf signal	Background	Corrected	Tf signal	Background	Corrected	Tf signal	Background	Corrected
270.527013	199.470774	71.0562392	307.898051	255.83777	52.0602813	298.18776	247.517913	50.669847
216.021364	191.24691	24.7744536	534.819246	273.520626	261.29862	421.620797	259.611457	162.009339
225.960869	187.769207	38.1916624	352.109405	271.572738	80.5366671	525.067093	275.33099	249.736102
223.6437	191.168308	32.4753919	422.855287	268.70876	154.146527	404.222876	264.124944	140.097932
240.177945	197.368701	42.8092434	526.585492	267.44094	259.144551	317.201097	265.283698	51.9173991
223.787773	196.606216	27.1815571	326.276981	268.906205	57.3707761	354.472614	257.252472	97.2201413
211.061524	195.937614	15.12391	336.227911	247.643988	88.5839226	281.166984	263.821168	17.3458156
285.609647	202.17503	83.4346177	562.718023	264.388187	298.329836	545.337859	265.13532	280.202539
319.135188	204.516947	114.618241	526.355311	279.857909	246.497402	279.489983	247.529167	31.9608164
291.465779	203.171943	88.293836	481.368734	277.767392	203.601343	329.179929	279.043807	50.1361218
227.405588	196.658576	30.747012	418.053302	264.294802	153.758499	368.099377	287.520689	80.5786888
273.039846	197.471913	75.567933	520.491879	281.689409	238.80247	418.60365	283.052773	135.550878
227.676158	198.695485	28.9806723	725.054756	292.028804	433.025953	296.116309	272.594014	23.5222947
310.921808	199.040633	111.881175	342.69834	269.357722	73.3406181	368.292317	296.640416	71.6519005
329.087392	199.745067	129.342325	722.31927	303.038324	419.280946	313.839668	287.690597	26.149071
325.985932	202.776398	123.209534	365.881844	251.106091	114.775753	348.65734	282.90712	65.7502206
303.677856	201.608826	102.06903	342.563364	243.340556	99.2228087	324.305968	286.770399	37.5355684
305.582946	193.846737	111.736209	297.669645	250.079745	47.5899006	389.365908	292.704202	96.6617058
277.370995	267.047632	10.323363	370.522424	253.168417	117.354007	314.635338	288.075947	26.5593912
329.228269	276.67244	52.5558294	539.232728	254.509029	284.7237	302.14597	277.028904	25.1170662
291.481791	281.910248	9.57154212	740.690224	270.793639	469.896585	368.235532	270.454079	97.7814532
309.974519	285.053016	24.9215029	385.107082	254.47228	130.634803	328.777435	275.477417	53.3000174
380.338358	288.081158	92.2572005	759.793115	288.559912	471.233203	445.845563	277.09124	168.754323
311.20289	284.48712	26.7157704	765.506649	267.375435	498.131214	534.611116	313.190433	221.420683
314.588837	283.180035	31.4088025	290.219871	244.393147	45.8267239	323.518369	302.143756	21.3746136
299.169318	285.910917	13.2584012	583.363392	290.711277	292.652115	571.593062	338.558758	233.034304
320.984716	278.742652	42.2420641	752.483352	257.612768	494.870584	379.215239	316.200939	63.0143
291.903978	273.07962	18.8243582	605.705147	240.238286	365.466861	411.69931	322.19736	89.5019505
311.865041	258.063849	53.8011916	333.264269	212.922133	120.342136	395.281697	309.562846	85.7188511
317.344201	274.748193	42.5960088	576.087851	233.959789	342.128063	365.18531	320.924761	44.2605489
306.910005	275.862761	31.0472436	305.344442	216.243535	89.1009066	484.290122	322.056405	162.233716
332.822617	274.593362	58.2292545	508.45768	230.659728	277.797952	369.286934	315.739937	53.5469972
316.434873	283.666085	32.7687881	249.85369	214.239243	35.6144462	366.540495	335.080743	31.4597517
301.136478	280.808377	20.3281001	248.20127	196.615315	51.5859552	682.353022	345.125028	337.227995
322.66434	278.591551	44.0727891	256.09504	203.378822	52.7162184	331.73847	329.167281	2.57118897
297.061457	264.237987	32.8234699	561.548287	209.296137	352.252149	421.569698	347.413535	74.1561633
323.003802	273.542228	49.461574	349.850106	221.123158	128.726948	571.021838	342.877755	228.144083
321.657315	277.6991	43.9582149	421.472867	222.62335	198.849517	463.555455	360.269772	103.285684
295.111735	284.313505	10.7982302	579.987291	232.891397	347.095894	434.58454	360.08541	74.4991301
295.079785	287.06964	8.01014523	273.186964	230.1948	42.9921639	549.715193	368.631464	181.083729
297.655363	286.472762	11.1826011	362.610993	243.257201	119.353793	394.304326	366.045671	28.258655
314.842956	279.825539	35.0174173	270.244238	210.204832	60.0394065	369.846281	343.532459	26.3138218
283.503671	268.304394	15.1992765	333.347274	217.350429	115.996846	397.938942	360.525961	37.4129808
286.783833	264.197641	22.5861923	283.427531	234.508666	48.9188651	376.154727	355.099136	21.0555911
302.163543	269.87171	32.2918331	275.043757	233.051081	41.9926755	515.567764	370.928684	144.63908
306.631931	275.414341	31.2175892	705.877268	238.326194	467.551074	449.781633	346.985079	102.796553
340.009019	259.754924	80.2540956	350.963646	227.040899	123.922747			
271.998745	262.179116	9.8196288	298.887651	227.831518	71.0561323			
			563.720679	244.149112	319.571567			
			366.481103	229.013987	137.467116			
			580.596634	261.257964	319.33867			
			306.839855	258.587289	48.2525663			
			636.904073	252.959962	383.944111			
			452.088293	245.698578	206.389715			
			322.987124	232.208649	90.7784752			
			732.011736	251.845656	480.166081			
			307.210517	225.64119	81.5693262			

BES7 2GPI

15sec			**60 sec**			**600 sec**		
Tf signal	Background	Corrected	Tf signal	Background	Corrected	Tf signal	Background	Corrected
247.892737	182.852743	65.0399943	390.966746	225.475361	165.491385	606.63885	278.712675	327.926174
265.317564	184.88521	80.432354	467.652758	235.807767	231.84499	522.836779	278.919319	243.917461
237.91247	187.100238	50.8122317	739.189223	237.932359	501.256864	321.81492	268.368939	53.4459805
349.815799	188.069739	161.74606	565.400342	238.383329	327.017013	502.131997	273.638099	228.493898
293.908391	185.158769	108.749621	358.14173	224.732379	133.409351	500.773485	281.696054	219.077431
303.537896	188.214237	115.323658	287.355536	218.453149	68.9023869	357.373859	284.06719	73.3066693
242.402414	180.268968	62.1334459	630.247598	216.679795	413.567803	634.464334	293.587598	340.876736
282.917481	183.412698	99.5047824	430.27931	226.177157	204.102152	434.644566	288.377967	146.266599
244.126259	177.528166	66.598093	687.079315	247.523684	439.555631	358.443243	285.289154	73.1540891
318.052266	185.544796	132.507471	422.426521	229.018606	193.407915	705.008599	305.744685	399.263914
279.258024	177.741175	101.51685	323.106905	230.680488	92.4264168	407.802718	296.756594	111.046123
282.688793	180.297829	102.390965	817.271614	257.465417	559.806198	466.453458	284.082256	182.371202
307.713726	174.543191	133.170536	867.563407	245.309834	622.253574	411.330661	282.330703	128.999957
292.107308	180.116052	111.991256	784.141016	245.229815	538.9112	431.445288	265.008617	166.43667
234.642611	183.174794	51.4678169	915.109666	243.715578	671.394087	392.929535	244.140749	148.788786
256.771796	174.754545	82.0172507	576.869554	232.767271	344.102283	349.663426	255.51432	94.1491061
183.015015	168.348667	14.6663484	282.631245	210.943455	71.6877898	402.318674	241.763086	160.555588
277.032718	180.659628	96.3730898	279.903678	215.002284	64.901394	461.522451	268.549529	192.972921
257.322826	182.675541	74.6472853	387.094495	222.026336	165.06816	299.033233	261.283131	37.7501019
308.787712	187.524502	121.263211	339.57099	222.221949	117.349041	570.972593	269.795767	301.176826
188.163359	170.861471	17.3018883	656.628219	225.900496	430.727722	324.881755	258.292578	66.5891767
283.090492	199.312376	83.7781155	292.256795	223.84274	68.4140545	307.397299	262.124661	45.2726388
275.194135	198.538112	76.6560227	756.774718	261.302958	495.471759	322.427194	262.43369	59.9935046
333.272019	204.537505	128.734515	778.719406	232.517286	546.20212	451.68599	267.762544	183.923446
336.273948	202.756249	133.517699	598.660111	250.438023	348.222088	512.897845	249.290844	263.607001
300.131576	199.191786	100.939789	751.243739	258.717666	492.526073	509.51501	265.966233	243.548777
245.76248	200.218599	45.5438811	267.322421	226.966652	40.3557686	505.998385	270.275011	235.723375
273.39596	199.691615	73.704345	652.027004	246.496777	405.530227	563.237246	265.448661	297.788585
282.490435	196.436319	86.0541155	750.890727	249.877863	501.012864	550.74409	277.333799	273.410292
274.613809	199.458397	75.155412	450.811048	239.320912	211.490135	438.783627	261.282862	177.500765
338.689708	201.074637	137.61507	569.373968	249.068349	320.305619	555.228376	293.668578	261.559798
217.80695	196.792091	21.0148588	879.97008	243.141119	636.828961	721.591486	297.402217	424.18927
263.018576	199.732067	63.2865092	413.652013	278.43827	135.213743	387.920953	297.793329	90.1276244
249.496214	201.909242	47.5869727	322.634058	247.285841	75.3482165	369.137846	292.230747	76.9070994
316.877652	203.655118	113.222534	467.523137	249.116628	218.406509	503.786275	304.376169	199.410106
249.051887	202.983385	46.068502	819.823657	264.035084	555.788573	724.061185	304.643939	419.417245
281.69944	199.869956	81.8294843	678.35576	251.108023	427.247737	599.991469	315.178645	284.812824
266.194573	196.270174	69.9243994	322.547824	233.310124	89.2376992	416.201399	295.573689	120.62771
334.04686	203.385998	130.660861	801.099412	250.466419	550.632992	555.293517	309.033704	246.259813
299.349789	198.417214	100.932575	387.942382	242.532124	145.410258	596.003991	308.772722	287.23127
205.657151	191.041912	14.6152391	310.612123	215.097435	95.5146882	797.167341	311.801052	485.366289
289.521839	206.504662	83.0171762	721.486946	240.409111	481.077835	751.143348	303.746017	447.397331
227.34385	210.638597	16.705253	555.552117	235.715747	319.83637	552.304002	305.079011	247.22499
308.169623	208.847566	99.322057	703.015298	250.441654	452.573644	617.449004	292.164119	325.284885
262.07769	213.204104	48.8735866	361.444873	222.451855	138.993018	381.620313	279.732202	101.888111
267.468023	210.384198	57.0838249	329.944877	227.018772	102.926104	378.36234	290.088508	88.2738312
226.953046	211.141426	15.8116199	753.20834	232.552997	520.655344	437.47037	276.072788	161.397581
269.70887	207.039641	62.6692283	601.202009	244.113821	357.088188	435.313585	281.385836	153.927749
214.52326	204.283009	10.2402507	553.991433	233.478713	320.512719	340.448513	264.601207	75.8473066
243.931658	211.751512	32.1801461	276.938485	226.345573	50.5929123			
290.335054	213.014949	77.3201044	801.120032	240.220535	560.899497			
266.537327	201.642545	64.8947814	461.986787	220.874465	241.112321			
343.287173	205.822294	137.464879	563.446804	224.556551	338.890253			
216.982971	206.579469	10.4035027	693.986995	238.446832	455.540162			
249.042373	205.788136	43.2542373	624.868348	214.203814	410.664534			
229.234525	204.736721	24.4978039	312.007538	231.587357	80.4201808			
243.635383	205.122937	38.5124466	598.482561	212.61358	385.868981			

Table S3
BES1-1 GPI

15 sec			**60 sec**			**600 sec**		
Tf signal	Background	Corrected	Tf signal	Background	Corrected	Tf signal	Background	Correced
234.775782	203.873377	30.9024048	430.576336	283.904626	146.67171	270.642614	242.393419	28.2491948
304.145806	202.660483	101.485323	427.849424	292.333524	135.515899	287.451875	240.639326	46.812549
214.218142	197.734326	16.483816	391.214386	298.413111	92.8012754	534.720136	257.636665	277.083471
291.23726	207.828409	83.4088513	358.875593	288.150767	70.7248261	277.984139	240.199136	37.7850026
261.148777	197.274474	63.8743035	414.639075	285.790569	128.848506	587.766636	250.113912	337.652724
220.735959	203.537313	17.1986453	414.424537	302.779975	111.644561	286.882546	254.604694	32.2778512
257.353716	193.027339	64.3263775	321.398208	292.160018	29.2381899	271.128827	249.529625	21.5992017
286.7046	247.012705	39.6918959	440.18949	299.598491	140.590999	277.848127	259.932282	17.9158458
271.928127	245.256637	26.6714894	356.546342	274.067394	82.4789482	388.457951	249.883058	138.574893
316.794736	258.311931	58.4828052	348.675102	282.865474	65.8096285	433.709883	253.86544	179.844443
268.456657	245.33976	23.1168969	345.528921	281.680444	63.848477	472.246897	239.098758	233.148139
297.862268	254.079599	43.7826682	394.034437	281.685222	112.349215	262.824643	249.630857	13.1937853
261.914497	244.681209	17.2332873	385.309148	278.705608	106.60354	520.444459	255.411644	265.032814
267.797693	241.958001	25.8396917	363.551895	281.644037	81.907858	547.705794	289.539683	258.166111
269.838301	255.565208	14.2730923	443.176529	263.135972	180.040557	537.976087	278.975919	259.000168
314.205674	246.193758	68.0119163	349.053596	273.279592	75.7740033	402.977283	291.006563	111.97072
249.678541	237.186589	12.4919523	421.862759	267.595096	154.267663	391.668459	300.948794	90.7196652
263.778742	247.94747	15.8312723	398.075086	226.932226	171.14286	397.115995	303.76716	93.3488352
301.326998	274.136265	27.1907331	351.621831	220.223631	131.3982	567.662969	291.537451	276.125518
272.657941	250.799173	21.8587675	470.560685	233.376129	237.184556	432.437619	292.397987	140.039632
271.73915	249.966658	21.7724924	302.103221	230.452781	71.6504402	619.407966	285.106685	334.301282
357.304406	334.772627	22.5317799	291.686809	222.739557	68.947252	402.32142	342.111073	60.2103475
341.010476	323.146652	17.8638236	425.499256	223.205339	202.293917	453.868563	360.021989	93.8465745
338.43351	325.604066	12.8294439	506.685785	215.680521	291.005264	405.981197	350.033441	55.9477564
343.671106	332.412443	11.2586625						
352.478644	322.30651	30.1721341						

BES1-2 GPI

15sec			**60 sec**			**600 sec**		
Tf signal	Background	Corrected	Tf signal	Background	Corrected	Tf signal	Background	Correced
218.399832	191.124987	27.2748454	724.43953	217.917581	506.521949			
294.154852	196.544623	97.6102287	548.99508	212.350592	336.644488	541.016991	262.699051	278.31794
212.136693	195.214351	16.9223422	314.431469	204.743319	109.68815	285.584734	260.479405	25.1053299
262.848476	194.241362	68.6071136	492.191051	210.504542	281.686509	523.488474	264.453981	259.034492
299.164106	194.355854	104.808253	445.269671	209.295051	235.97462	418.35013	270.350725	147.999405
248.558701	197.284171	51.2745293	447.533955	207.612561	239.921394	515.089333	249.04283	266.046503
335.442985	195.705871	139.737113	748.321073	206.81923	541.501843	698.288118	275.387093	422.901025
223.67045	192.648126	31.0223234	737.923592	205.295989	532.627603	373.834541	274.222351	99.6121898
213.017357	188.502244	24.515113	618.600222	207.961365	410.638857	297.319077	274.597894	22.7211826
245.347943	182.301101	63.0468418	557.782201	198.055422	359.726779	302.421563	278.956335	23.4652277
222.28335	187.05765	35.2257004	475.835383	207.339708	268.495674	392.204996	275.514891	116.690105
262.664858	190.868765	71.7960929	675.614144	210.883379	464.730765	298.669704	274.819244	23.8504597
222.551139	191.517776	31.0333628	370.293466	209.769431	160.524036	281.714589	266.892605	14.821984
240.715427	187.335455	53.3799722	437.232891	193.668192	243.564699	621.809336	273.515719	348.293617
264.645648	186.379458	78.26619	257.117092	196.785309	60.331783	286.954908	273.528366	13.4265421
279.265136	190.411315	88.8538216	643.597643	243.528223	400.06942	433.496754	266.8967	166.600054
268.783581	194.517592	74.2659891	527.445209	240.96208	286.483128	420.19317	273.223489	146.96968
242.429856	198.959583	43.4702732	467.698995	229.328577	238.370418	290.177674	262.666819	27.5108543
282.006158	194.093792	87.9123662	263.909656	217.802492	46.107164	341.553629	263.003851	78.5497775
249.620311	199.163133	50.4571789	330.397118	239.601499	90.7956182	426.453288	277.979573	148.473715
236.263425	197.902823	38.3606027	748.09636	239.377204	508.719156	466.51363	275.520429	190.993201
279.750019	193.188704	86.5613153	436.886298	249.448428	187.43787	491.687534	264.245959	227.441575
292.408658	195.500198	96.9084602	273.319074	258.868209	14.450865	429.519163	267.60496	161.914202
			376.5206	257.25119	119.269411	328.923152	273.940557	54.9825955
			720.093001	230.73258	489.360421	320.968958	266.208676	54.7602827
			795.160401	241.603944	553.556457	296.599195	279.496228	17.1029671
			378.107244	221.609327	156.497917	445.503247	280.268316	165.234931
			348.53209	237.285133	111.246958	469.347182	277.758576	191.588606
			358.095546	236.25002	121.845526	296.463426	270.560027	25.9033986
			511.25555	222.830525	288.425026	514.763865	264.364088	250.399778
			261.156128	231.916574	29.2395536	509.202331	275.454572	233.747759
			759.169984	221.642662	537.527322	504.4988	270.451083	234.047718
			784.147973	216.540623	567.60735			
			277.338981	233.243562	44.0954191			

Table S4

BES1-1GPI

FI of cell	FI backgroun	Corrected
4169.1891	1369.28354	2799.90556
5517.00505	1518.63807	3998.36698
4466.68632	1366.80352	3099.8828
4454.89058	1355.07642	3099.81416
3703.71709	1403.40315	2300.31394
3883.55348	1423.43266	2460.12082
4161.70658	1313.01821	2848.68837
5345.77071	1237.77552	4107.99519
3812.64022	1395.97521	2416.66501
5233.52321	1460.97417	3772.54904
4416.26956	1305.2035	3111.06606
5690.69117	1456.09166	4234.59951
4974.73575	1634.37369	3340.36206
4159.68304	1728.30496	2431.37808
5966.39615	1562.48411	4403.91204
6844.52143	1658.0438	5186.47763
4849.82735	1290.27353	3559.55381
4387.01769	1368.57291	3018.44478
4039.22212	1581.33536	2457.88675
5653.91974	1854.64047	3799.27927
6128.88791	1760.47869	4368.40921
5461.04714	2209.05985	3251.98729
4121.67164	2404.91355	1716.75809
4697.11634	1529.9975	3167.11885
4032.46619	2088.2814	1944.1848
4472.13665	1651.82691	2820.30974
4666.65855	1196.71066	3469.94789
6836.58984	1242.24821	5594.34163
4340.12546	1147.18195	3192.94351
4544.95411	1208.12037	3336.83374
4244.87746	1238.19354	3006.68392
3591.7771	1674.24542	1917.53168
4342.65985	1209.49804	3133.16182
4607.30645	1101.59142	3505.71503
4303.83696	1400.3393	2903.49766
4061.93873	1506.87737	2555.06135
4602.69081	1395.39691	3207.29391
4478.11811	1502.67812	2975.43999
4903.37558	1312.0718	3591.30378
3691.56141	1389.23716	2302.32425
3363.79062	1299.70141	2064.08921
3387.93578	1428.83978	1959.096
3595.42411	1487.81455	2107.60956
3073.78033	1375.52312	1698.25722
2946.87813	1334.96877	1611.90936
3583.73492	1531.62643	2052.1085
4565.25277	1370.67542	3194.57735
3289.89102	1503.71898	1786.17204
3901.68966	1475.30914	2426.38053
4489.0743	1677.21025	2811.86405
3344.62854	1442.39829	1902.23025
3226.46594	1737.63654	1488.82939
4014.50712	1757.63624	2256.87088
4816.73036	1683.81031	3132.92006
3354.05243	2063.54544	1290.50699
3515.58823	1466.18232	2049.40591
3846.69126	1294.55445	2552.13681
3776.52195	1309.98233	2466.53962
3469.76282	1414.831	2054.93182
4986.73253	1276.04999	3710.68253
3775.15461	1180.49606	2594.65855
4504.38413	1081.42983	3422.9543
2792.16911	1034.30053	1757.86859
3021.98636	1350.46996	1671.5164
3434.43803	1301.40369	2133.03433
3546.77908	1272.6147	2274.16437
3986.38403	1438.23311	2548.15092

BES1-2GPI

FI of cell	FI backgroun	Corrected
7397.90542	1601.33761	5796.56781
5194.63503	2016.5935	3178.04153
5046.05	1414.73603	3631.31397
7014.50272	1602.20093	5412.3018
9167.4573	1671.26481	7496.19249
4705.50447	1980.2286	2725.27587
5314.19549	1671.40467	3642.79082
5140.15445	1549.04497	3591.10948
6865.54536	1434.11577	5431.42959
5011.45679	1530.49063	3480.96617
5880.58125	1596.30831	4284.27294
5714.74356	1723.14111	3991.60244
4558.88611	1614.53589	2944.35022
6957.89341	1697.69679	5260.19663
4531.5057	1858.15333	2673.35237
4075.3613	1559.91582	2515.44548
6386.4478	1525.08275	4861.36505
4768.65125	1532.22332	3236.42793
5121.03961	1810.44301	3310.5966
4289.88786	1661.7653	2628.12256
4224.13117	1657.07444	2567.05673
4022.22367	1542.06811	2480.15556
4757.77671	1640.24423	3117.53248
3972.69131	1458.73595	2513.95536
4952.72435	1439.38026	3513.34408
4829.96955	1417.7771	3412.19246
4799.97044	1399.56123	3400.40921
6406.86227	1455.44769	4951.41458
5247.45768	1510.92269	3736.53499
4812.53749	1432.02822	3380.50926
3891.33291	1322.36933	2568.96358
4230.59221	1453.39171	2777.2005
5191.87406	1473.93191	3717.94215
4181.71502	1518.48565	2663.22938
5322.50447	1662.18291	3660.32157
5375.1074	1330.79175	4044.31565
5076.07008	1336.94676	3739.12332
5146.07223	1568.86249	3577.20975
3651.2423	1499.63945	2151.60285
4230.18298	1501.29572	2728.88725
4648.14714	1444.06839	3204.07874
4921.54447	1618.38973	3303.15474
5262.78448	1663.90231	3598.88217
5094.47869	1515.9482	3578.5305
5069.50906	1799.36771	3270.14136
4622.10492	1412.16133	3209.94359
4646.93306	1466.65244	3180.28061
4191.70167	1302.97995	2888.72173
3250.59116	1610.00582	1640.58534
5114.45282	2225.04777	2889.40506
4169.27925	1557.3028	2611.97645
5792.44183	1510.41649	4282.02534
4092.54011	1577.27939	2515.26071
3919.93385	1439.58637	2480.34748
3929.92664	1387.49081	2542.43583
3469.22981	1284.5608	2184.66901
3484.57208	1504.05021	1980.52186
6399.72065	1424.07604	4975.6446
5678.3475	1760.17238	3918.17512

BES7-1 GPI

Cell FI	Background F	Corrected
12837.0266	4681.34276	8155.68384
17856.946	5163.70588	12693.2401
14578.6019	6733.43986	7845.16204
8257.59879	4489.82684	3767.77196
21507.8573	6313.37498	15194.4824
9684.06919	6390.32598	3293.7432
11574.0715	2055.70618	9518.36528
14178.8166	3363.52103	10815.2956
9229.06276	3063.70515	6165.35761
11373.0827	2629.73056	8743.35219
9459.26121	3335.64905	6123.61216
16907.3104	5001.21501	11906.0954
12640.7288	3904.67238	8736.05641
9608.94197	4574.54556	5034.39641
21016.9562	4752.91193	16264.0443
18762.9114	5075.52375	13687.3876
10587.7768	4418.42652	6169.35031
6315.10407	3887.97902	2427.12505
5872.17781	4196.63916	1675.53865
6740.69995	4107.35088	2633.34907
22877.5275	5306.45609	17571.0714
8086.627	5258.43577	2828.19123
12070.3399	4203.20336	7867.13658
11069.5206	3399.07264	7670.44792
8798.09693	3788.9649	5009.13203
8394.35496	3715.74066	4678.6143
8378.80007	4547.47284	3831.32724
7918.69538	3390.73456	4527.96082
11517.9798	3080.5122	8437.46759
10405.1445	3515.78948	6889.35503
9353.17874	2897.44106	6455.73768
15463.0206	3867.05777	11595.9629
8263.89373	2437.17601	5826.71772
7236.70061	3213.57139	4023.12922
4703.99833	2573.29191	2130.70642
14961.5196	3747.41527	11214.1043
13139.3319	3888.15671	9251.1752
17608.9766	4108.78449	13500.1921
10541.4171	3529.86644	7011.5507
7598.97705	3195.20233	4403.77473
15210.038	3511.77355	11698.2644
6002.27436	1336.80393	4665.47044
7559.97018	1619.01031	5940.95988
11302.1653	1938.84383	9363.32151
11072.582	1652.44181	9420.14021
4273.02183	1673.77179	2599.25004
10248.0598	1698.39438	8549.66537
6818.36613	1502.03382	5316.33231
7678.34762	1599.25187	6079.09574
13070.9653	2013.20888	11057.7564
5902.91196	1489.5861	4413.32586
6371.34498	1500.68632	4870.65866
8271.58377	1379.03512	6892.54865
11719.5397	1918.39672	9801.14298
11442.8635	1962.45823	9480.40524
3919.90251	1285.24344	2634.65907
8493.24379	1627.55856	6865.68524
10624.4969	4166.08267	6458.41427
8933.71896	3393.76976	5539.9492
12578.264	3328.29907	9249.96496
9401.38217	3636.60645	5764.77571
17873.1515	4066.34463	13806.8069
14654.5717	2931.92614	11722.6456
8199.72123	2538.99357	5660.72766
10690.3571	2804.71569	7885.64144
17867.1895	3092.72876	14774.4608
6417.39227	2788.89755	3628.49472
6908.05726	2958.14219	3949.91507

BES7-2GPI

Cell FI	Background F	Corrected
14596.8045	3396.05044	11200.7541
12827.5242	3393.0242	9434.49997
12743.1915	3332.9112	9410.28027
12563.7286	3331.35159	9232.37704
11161.5916	3277.68613	7883.9055
10628.5005	3184.04184	7444.45867
10364.0054	3162.29286	7201.71257
9940.49315	3076.5333	6863.95985
9574.09572	3051.88258	6522.21314
9342.3204	3027.09073	6315.22967
9010.88678	3011.91133	5998.97545
8607.00698	2963.3325	5643.67447
7853.71566	2955.74043	4897.97523
7065.93033	2879.59719	4186.33315
6760.38553	2828.94613	3931.4394
6125.49891	2805.08647	3320.41244
5915.60049	2774.39108	3141.20941
13164.126	4607.8443	8556.28172
14804.4068	4590.81764	10213.5892
12044.1318	5208.19234	6835.93951
19551.6645	5003.8709	14547.7936
15227.5612	5833.93699	9393.6242
14260.7814	4752.39096	9508.39049
19235.7898	4988.06845	14247.7214
9781.47423	4129.59609	5651.87814
13489.69	3658.64074	9831.04925
16104.6728	4310.65582	11794.0169
15238.7876	4766.47593	10472.3117
11790.272	3839.99295	7950.27903
15302.1429	3715.72763	11586.4152
7879.73013	3866.95582	4012.77431
10672.888	3674.82336	6998.06459
10890.1711	3531.50056	7358.67057
10747.2814	4092.10536	6655.17607
12120.564	3893.12971	8227.4343
10693.786	3313.44112	7380.34485
11334.7401	4036.58485	7298.15529
9852.47699	4077.37446	5775.10253
13146.5762	4806.09194	8340.4843
12910.7939	4896.15198	8014.6419
9639.8082	3884.35938	5755.44881
14823.3155	5220.65122	9602.66426
12602.9559	4471.4112	8131.54473
10275.7252	4019.51278	6256.21245
12437.123	3568.66638	8868.45659
11381.6733	4956.19825	6425.47509
12961.427	3769.22951	9192.19746
28652.0939	7790.18995	20861.904
39810.3447	7348.82936	32461.5154
11230.3035	5746.28909	5484.01436
34734.4885	8056.44612	26678.0424
10087.011	6371.82538	3715.18559
22591.4696	7408.2788	15183.1908
29298.3307	6245.77872	23052.552
17178.1426	5795.58891	11382.5537
30589.019	8105.09675	22483.9222
10660.4765	5307.62018	5352.85631
23269.3716	4672.84322	18596.5283
15321.0247	5381.674	9939.35071
18432.5793	6361.81345	12070.7658
22047.3234	5155.23628	16892.0871
44621.7256	10497.3445	34124.3811
14672.1238	6648.39164	8023.7322
25233.7494	9511.99941	15721.7499
28621.3122	9511.99941	19109.3128
21952.2258	8968.63297	12983.5928
17127.1369	9357.45498	7769.6819
41312.7102	12880.4142	28432.296

20683.4922	3047.92127	17635.5709
6095.30543	2798.56066	3296.74476
14839.6706	2914.04669	11925.6239
13068.3758	3060.76952	10007.6063
6706.24789	3121.48318	3584.76471
16044.9009	4262.1351	11782.7658
15395.3617	6158.93497	9236.42676
13498.7991	3595.3978	9903.40131
9703.24426	3741.26092	5961.98334
19649.345	4109.21333	15540.1317
17432.3565	4652.47975	12779.8767
15859.6605	3661.14234	12198.5181
17979.2955	5041.82697	12937.4685
16472.5519	3590.97316	12881.5787
14309.8958	4121.26972	10188.6261
16235.584	4150.48332	12085.1007
17900.6796	4531.93406	13368.7456
14657.4608	3777.59456	10879.8662
15432.3774	4341.38168	11090.9957
20632.1338	3979.56919	16652.5646
17866.4617	4037.67044	13828.7912
17459.0386	4786.22063	12672.8179
9560.24487	3368.6286	6191.61627
4606.1829	2927.84182	1678.34108
4596.79703	3020.6873	1576.10974
6663.79374	2985.62929	3678.16445
7239.77317	3475.27868	3764.49449
8663.68838	3501.51167	5162.17672

21815.4615	9429.58456	12385.877
7354.70445	3872.3488	3482.35565
27227.0988	7005.97022	20221.1286
20877.738	8990.7165	11887.0215
26307.1804	8765.73706	17541.4433
32094.9278	7321.51356	24773.4142
13807.2987	6878.01313	6929.28559
37369.6264	9009.61228	28360.0142
31935.4964	9140.15698	22795.3394
16396.7827	8824.2721	7572.51062
40337.0674	10206.0609	30131.0065
18377.9973	10058.169	8319.82832
37444.5905	9070.05294	28374.5376
22141.4275	7954.17203	14187.2555
22922.965	7011.73101	15911.234
24585.2531	7588.65098	16996.6021
13685.735	7217.58968	6468.14533
36560.9886	9776.42725	26784.5613
18183.3487	11097.7722	7085.57648
20765.1325	9151.99895	11613.1335
9734.20179	7437.75866	2296.44313
10807.2598	8079.42412	2727.83565
20203.9132	8409.65566	11794.2575
16519.0085	7678.60639	8840.40211
18698.6301	6087.98564	12610.6445
13361.1002	4958.97028	8402.12994
9484.52546	4920.36035	4564.16511
22564.3954	6224.63287	16339.7625
10647.0543	6146.32952	4500.72476
26330.8566	8926.81754	17404.039
33165.9144	9949.59197	23216.3224
25891.9188	8903.45542	16988.4633
10112.603	6528.53747	3584.0655
36326.5213	8593.36712	27733.1542
35099.0257	7446.47981	27652.5459

Table S5. Oligonucleotides

		Forward	Reverse	Template
BES7-ESAG7 + GPI anchor	PacI-EcoRI	TGATTAATTAAGGTCTTGCGCT	GTGGAATTCATCTTGTTCAATCAT	BES7 gDNA
	EcoRI-PacI	ATCGCCTTCTTGACGAATTCTT	CAATTAATTAAGCGCATCAACTTGCACC	BES7 gDNA
Blast R	EcoRI-EcoRI	CCCGAATTCTAGATGCCTTTGTCTCAAGAAG	GCAGAATTCTTAGCCCTCCCAC	pPOT v7 Blast-Blast
BES7-ESAG7 no anchor	SacI-BsrBI	GTTGAGCTCACTAATGATCAGC	CCCCGCTCCCGTGAAAGGT	RT-PCR from Lister427 MiTat1.2 purified RNA
sgRNA templates	5' G418 resistance gene	GAAATTAATACGACTCACTATAGGGAATAGCCTCTCCACCCAAGGTTTTAGAGCTAGAAATAGC		
	ESAG7 3'UTR	GAAATTAATACGACTCACTATAGGAACGTGTGAAGCCTGAAATGGTTTTAGAGCTAGAAATAGC		
BES1-ESAG7 no anchor	PacI-BstEII	TGATTAATTAAGGTCTTGCGCT	GATGTCGAGCCCGACGCGCGTG	BES7 gDNA (contains G418 resitance gene in BES1 expression site)
	BstEII-PacI	CCACGCGCCACACCGTCGACCC	CAATTAATTAAGCGCATCAACTTGCACC	BES7 gDNA (contains G418 resitance gene in BES1 expression site)
BES1-ESAG7 + GPI anchor	SacI-BES7-ESAG7 stop	GGAGGCTGAGCTCACTAATGATCAGC	TCACAGCACTCCCAACAATAAAGCTGAAC	BES7-ESAG7 + GPI-anchor clone
	BES7-ESAG7 stop-PacI	AGGAAGGATGCGACAGAAGCTGC	CGTTGGGAGCTCTCCCATATGGTC	BES1-ESAG7 no anchor clone
sgRNA templates	5' UTR	GAAATTAATACGACTCACTATAGGAGTCATGCATGAACCGACAAGTTTTAGAGCTAGAAATAGC		
	ESAG7 3'UTR	GAAATTAATACGACTCACTATAGGAACGTGTGAAGCCTGAAATGGTTTTAGAGCTAGAAATAGC		
VSG221 in BES7 switch	KpnI-XhoI	GCTGGTACCCAAAGATTTGTTTTGAGGAG	CGCCTCGAGGCTTGGTTTTGCTGATCTTA	BES7(TAR153) DNA
	SpeI-SacI	CTTACTAGTATTTTTCCCCCTCAATTTTCCTT	AAAGAGCTCGTGAATCAAAAAAAAAAAATTAAATTC	BES7(TAR153) DNA